Front. Mech. Eng. 2023, 18(1): 8
https://doi.org/10.1007/s11465-022-0724-0

REVIEW ARTICLE

Advances in polishing of internal structures on parts made by laser-based powder bed fusion

Mingyue SHEN[a], **Fengzhou FANG** (✉)[a,b]

[a] *Centre of Micro/Nano Manufacturing Technology, University College Dublin, Dublin 4, Ireland*
[b] *State Key Laboratory of Precision Measuring Technology and Instruments, Laboratory of Micro/Nano Manufacturing Technology, Tianjin University, Tianjin 300072, China*

✉ *Corresponding author. E-mail: fengzhou.fang@ucd.ie (Fengzhou FANG)*

ABSTRACT The internal structures of metallic products are important in realizing functional applications. Considering the manufacturing of inner structures, laser-based powder bed fusion (L-PBF) is an attractive approach because its layering principle enables the fabrication of parts with customized interior structures. However, the inferior surface quality of L-PBF components hinders its productization progress seriously. In this article, process, basic forms, and applications relevant to L-PBF internal structures are reviewed comprehensively. The causes of poor surface quality and differences in the microstructure and property of the surface features of L-PBF inner structures are presented to provide a perspective of their surface characteristics. Various polishing technologies for L-PBF components with inner structures are presented, whereas their strengths and weaknesses are summarized along with a discussion on the challenges and prospects for improving the interior surface quality of L-PBF parts.

KEYWORDS laser-based powder bed fusion, polishing, internal structures, surface quality, surface features, post process, additive manufacturing

1 Introduction

Delicate internal structures, such as honeycomb with cellular structures and natural bone with gradient porosity, are designed to achieve specific functions in the nature. In contemporary industries, the demand for metallic parts with internal structures, such as conformal channels [1] and lattice structures [2], is high because of their light weight, high cooling efficiency, and superior energy absorption property [3,4]. However, applying traditional subtractive technologies to the fabrication of complex interior structures is difficult, time consuming, and costly [5,6]. Since the early technique of additive manufacturing (AM) became available in the late 1980s [7], AM processes based on material incremental approaches experienced rapid development in the following decades. Among various AM technologies, laser-based powder bed fusion (L-PBF), also known as selective laser melting, refers to a process in which a high-power laser beam is used to scan a powder bed. With the help of computer-aided design (CAD), desired models with intricate structures can be fabricated layer by layer until the entire component is finished. Given the advantages of L-PBF, such as geometric freedom and high material utilization ratio, it is widely utilized in the fabrication of various materials and is more preferred for the preparation of customized parts that require complex internal structures. Despite the advantages of this technology, L-PBF still faces an apparent limitation in terms of poor surface quality, which limits its applications in various industries.

The surface quality of L-PBF parts is generally inferior because of the adhesion of partially melted powders and the rough sintered area related to the behavior of the molten pool. Meanwhile, various effects also influence the final surface of L-PBF components. Owing to the same deposition approach, internal and outer surfaces on L-PBF parts actually possess similar surface qualities and features. Generally, surface roughness and surface features, such as the quantity of adhered powders could vary significantly with different deposition angles. Although the optimization of raw powders and process parameters could be helpful in reducing the balling phenomena and surface defects, eliminating the adhesion

Received March 7, 2022; accepted July 30, 2022

of powders and the unevenness of molten pool is difficult due to the use of powder bed and layer-by-layer deposition principle. In fact, the characteristics of surface features are relevant to L-PBF process and require further characterization that considers the differences in morphology, topography, microstructure, property, and bonding conditions. Furthermore, the complexity of surface and specific internal structure needs to be considered in analyzing the surface quality of L-PBF internal structures. Given that surface quality has significant influence on multiple functions, such as biological response, mechanical properties, and fluid dynamics, developing and applying appropriate polishing methods are crucial and in high demand to improve the surface quality of L-PBF components with internal structures.

Nowadays, numerous polishing technologies have been utilized to improve the internal surface quality of L-PBF parts. Compared with outer surfaces that could use various techniques, such as milling and blasting for surface finish, the use of proper polishing process to improve the quality of interior surfaces is more challenging. Traditional abrasive flow machining (AFM) has been applied to L-PBF internal surfaces [1]. In the meantime, techniques, such as abrasive fluid polishing (AFP) [8], electropolishing (EP) [9], and hybrid polishing technologies [10–12], are gradually applied to enhance the surface quality of L-PBF parts. Notably, these polishing methods have their own advantages and limitations in the polishing of L-PBF internal structures. Given the complexity of L-PBF surface features, investigating and establishing the relationship between L-PBF surface features and their corresponding material removal mechanisms of polishing are typically necessary. In comparison to outer surface, internal structures increase the difficulty of designing and establishing appropriate polishing equipment. Thus, more efforts should be devoted to the development of innovative polishing machines to improve the polishing efficiency and final surface quality of L-PBF internal structures.

The objective of this review is to present the surface characteristics and progress on the polishing of the internal structures of L-PBF metallic parts, as well as the research challenges and prospects. This work should be of great value to researchers who are interested in the state-of-the-art development of interior surface finish for L-PBF parts.

2 Process, internal structures, and applications

2.1 L-PBF process

As a type of laser additive manufacturing (LAM) technology, L-PBF was developed from laser sintering (LS). Table 1 summarizes various LAM technologies according to their mechanisms. In general, materials are partially melted in LS because of the low energy input of laser. Hence, low melting point materials are used as binders to bond un-melted solid cores with high melting point during LS. As a result, LS components usually possess low density and inhomogeneous microstructure, which means that a good combination of parameters and post-treatment, such as hot isostatic pressure are essential to LS products [7,13]. In comparison to LS, a more powerful laser is used in L-PBF. Therefore, L-PBF can deposit fully dense parts with better mechanical properties and surface finish. In terms of laser melting deposition (LMD), the powders are supplied by a coaxial feeding system that is completely different from the powder bed. Apart from powder supply, high power laser and large-size laser spot during LMD lead to large molten pools and result in surface roughness higher than that of L-PBF samples [7]. Thus, L-PBF is currently the preferred technology for manufacturing intricate components, especially those requiring complex internal geometries and good surface quality [5].

Different from conventional subtractive manufacturing techniques, L-PBF is based on a material incremental manufacturing philosophy. Several steps are followed from the creation of the virtual model to the completion of the three-dimensional (3D) object. In the first step, the CAD model of the product is produced mathematically. Then, specialized software slices this model into cross-sectional layers, generates the tool path, and sends the generated file to the L-PBF machine. Finally, the designed model could be fabricated layer-by-layer until the 3D component is completed. The schematic of the L-PBF apparatus is shown in Fig. 1. An L-PBF apparatus generally consists of a laser, an automatic powder spreading system, a computer for the process control, an inert gas protection system, and other accessorial systems, such as substrate and powder bed preheating system [7,14]. Before the printing process, the substrate is leveled and fixed on the building platform in the L-PBF machine. Then, the protective inert gas is fed into the

Table 1 Classification of various LAM processes

Process	Mechanism	Powder supply
LS	Partial melting of powder	Pre-spreading of powder before laser scanning (powder bed)
L-PBF	Complete melting of powder	Pre-spreading of powder before laser scanning (powder bed)
LMD	Complete melting of powder	Coaxial powder feeding with synchronous laser scanning

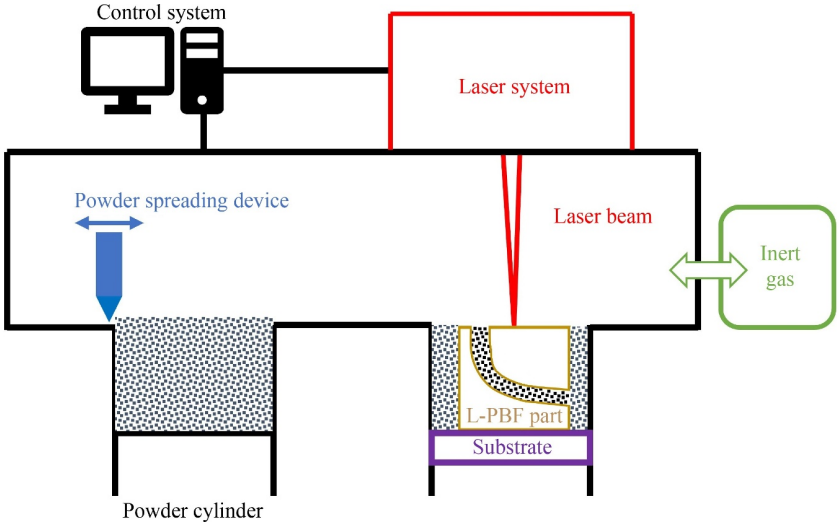

Fig. 1 Schematic of the L-PBF apparatus. L-PBF: laser-based powder bed fusion.

building chamber to reduce oxidation during L-PBF. After spreading a thin layer of powder on the substrate, the laser beam would melt the powders selectively according to the CAD model. Due to the alternate repetition of powder spreading and laser processing, powders on the top layer are fused onto the previously melted layer until the part is finished [15]. Given that the energy of the laser beam is high enough to melt the powder and form a molten pool, the rapid solidification of molten pools would leave sintered tracks on the L-PBF surface after laser scanning. Generally, L-PBF parameters, such as layer thickness, laser scanning speed, and hatch spacing, are adjusted for different printing materials [16]. In addition, the combination of various parameters is effective on the volumetric energy density of the laser-material interaction, which is important for the microstructure and properties of the final 3D products [17–20].

Based on the rapid melting and solidification mechanism, the printing process crucially relied on the behaviors of molten pool during L-PBF. As mentioned, a result of the interaction of powder bed and the high-powered laser is the formation of a molten pool. In general, the molten pool has a circular or segmental cylinder because of surface tension [21]. To reduce the surface energy, the molten area has the tendency to break up and therefore usually possesses an irregular geometry. Thus, the process parameters and the properties of raw powders influence the behavior of molten pool significantly because the molten region follows Plateau–Rayleigh instability [22]. In addition, the shape of the molten area is relevant to Marangoni convection [16]. Plateau–Rayleigh instability suggests that liquid cylinders with high aspect ratio tend to fracture to reduce surface energy. The breakup time of metals with a temperature above the melting temperature has a relationship with its geometry, surface tension, density, and viscosity [22]. Apart from Plateau–Rayleigh instability, Marangoni convection represents that the flow direction inside a molten pool depends on the gradient of fluid surface tension. If the flow is radially outward, then a shallow and wide molten region can be formed whereas a deep and narrow molten area is generated when the flow is radially inward [22]. After laser scanning, molten pool experiences rapid solidification and shrinkage with a cooling rate of 10^3 to 10^6 K/s [5]. The rapid cooling process results in phase transition in a non-equilibrium state, which affects the microstructure, mechanical properties, and surface morphology of the final L-PBF parts greatly. In this way, the L-PBF components can be fabricated through the melting, overlapping, and solidification of molten pools [23].

The principle and mechanism of L-PBF make it an effective technology for preparing fully dense parts with complex internal structures. Moreover, based on the complete melting/solidification mechanism [7], L-PBF has demonstrated the capability of manufacturing a wide range of materials, such as titanium [24,25], steel [26,27], cobalt chrome [28], aluminum alloys [29–31], nickel-based alloys [32,33], hard alloys [34,35], ceramics [36], and composites [37,38]. Due to the expanded degrees of freedom in the design of functional features, objects with desired geometry and intricate structures are allowed to be prepared by L-PBF for various applications [6].

2.2 Basic forms of L-PBF internal structures

The development of L-PBF technology has expanded the degrees of freedom in designing and manufacturing 3D objects with complex internal structures in one fabrication process. Industrial components with complex inner geometry and structures, such as hydraulic valve manifold [39], conformal cooling channels [1], and heat exchanger [40,41], are currently prepared by L-PBF for

various applications [42–44]. Despite the complexity of the interior structures of these products, they are usually composed of multiple basic forms. In general, channels (tubes) and cellular structures are the two basic forms of L-PBF internal structures.

L-PBF can fabricate straight and curve channels with different sizes and shapes of cross-section [45,46]. In terms of straight channels with different deposition angles in Fig. 2 [47], the inner diameter or size may change gradually, as indicated in Figs. 2(a) and 2(c) [47]. For a curve channel, the centerline of the channel is curved, where conformal channel is a passageway that follows the external shape or contour of the component [48,49]. In addition, the L-PBF is suitable for the preparation of complex channels, as depicted in Figs. 2(b) and 2(d) [47].

Due to the great potential for light-weighting, noise reduction, and energy absorption applications, L-PBF cellular structures have been investigated for many years to determine the relationship between geometry and their physical properties [5,50]. In general, cellular structure consists of stochastic foams and lattice structures. Notably, the porosity distribution in a stochastic foam is random. Apart from stochastic foams, L-PBF demonstrates unique superiority in fabricating periodic lattice structures [51] with various types of unit cells, such as face-centered cubic [52]. Furthermore, lattice structures with uniform and graded densities have been investigated (Fig. 3) [51]. Currently, the combination of the

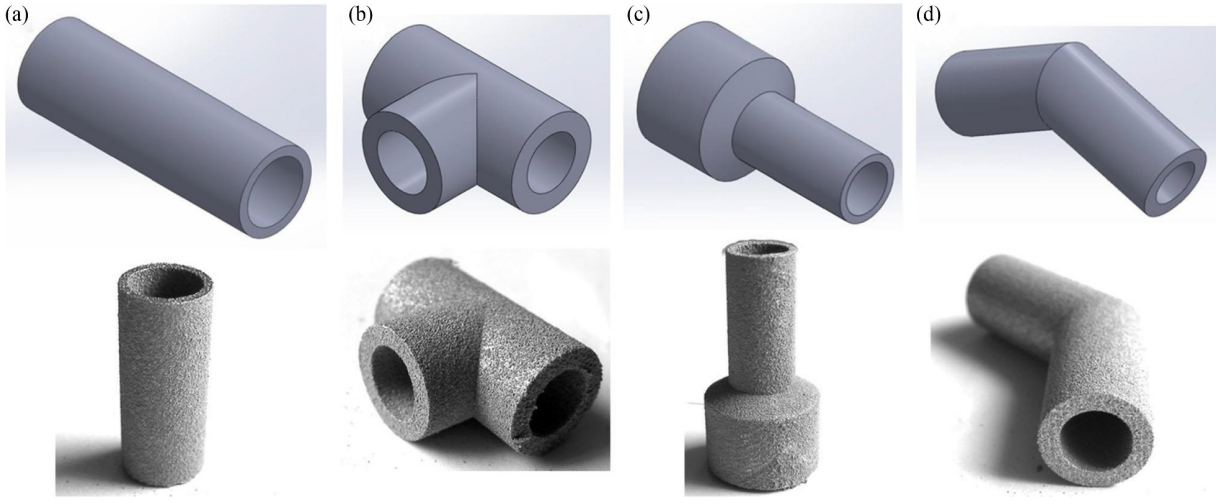

Fig. 2 Various laser-based powder bed fusion tubes: (a) straight, (b) horizontal T-shape, (c) vertical T-shape, and (d) reduction of size [47]. Reprinted with permission from Ref. [47] from Springer Nature.

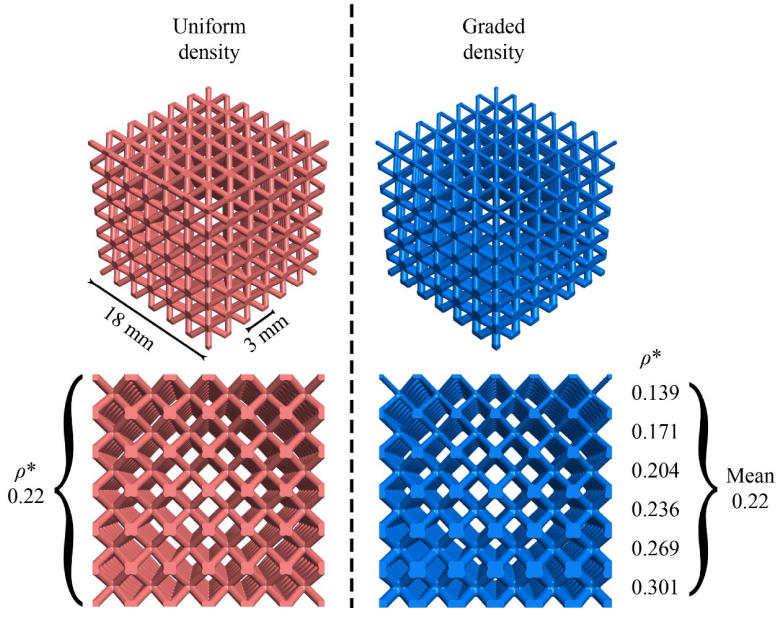

Fig. 3 Computer-aided design models of uniform (left) and graded density (right) lattice structures [51]. Reproduced with permission from Ref. [51] from Elsevier.

mechanical and functional properties of L-PBF cellular structures must be considered during the design and fabrication processes [53–55].

Maconachie et al. [56] reviewed the design, fabrication, and performance of L-PBF lattice structures and emphasized the importance of design and topography optimization. In fact, fabrication limitations, such as dimensional inaccuracies, are prone to occur particularly on L-PBF internal structures [57,58]. Thus, aspects, such as model design, raw powder size, melt pool size, deposition parameters, support structure, performance, and dimension prediction models, need to be considered for L-PBF internal structures [59,60]. Based on channels and cellular structures, L-PBF is used to manufacture components with various internal structures for applications.

2.3 Applications of L-PBF internal structures

L-PBF is becoming an effective process for manufacturing components with various internal structures for automotive, medical, and aerospace industries [61–65]. Given that straight channels are widely used, Romei et al. [40] analyzed the critical features of L-PBF heat exchanger and indicated that the control of feature size below 200 μm was achieved on 316L stainless steel. In Fig. 4 [66–68], the General Electric Company has applied L-PBF to prepare engine fuel nozzles with complex internal channels (Fig. 4(a)). For medical applications, Langi et al. [69] investigated the microstructure and mechanical properties of L-PBF 316L stainless steel tubes with thin wall thickness for stent applications. Moreover, straight channels with diameters of 200, 300, and 500 μm were designed and prepared by L-PBF on drug-delivering implants to reduce or avoid infection [70]. Apart from straight channels, conformal channels manufactured by L-PBF exhibit excellent cooling uniformity and efficiency in hydraulic [71] and mold [72] industries, as illustrated in Fig. 4(b) [67]. The current focus of L-PBF manifolds with curve channels is to investigate the relationship between microstructure and mechanical properties [71]. In terms of cellular structures, Yan et al. [73] fabricated L-PBF Ti–6Al–4V with different lattice structures for bone implant and found that the modulus and porosity of the lattices could be tailored to mimic human bones. Xiao et al. [68] designed three types of topology-optimized lattice structure, as shown in Fig. 4(c) [68], and tested their energy absorption efficiencies. Except for uniform lattice structures, Maskery et al. [51] also prepared and examined the mechanical behavior of graded L-PBF AlSi10Mg lattices in Fig. 3 [51]. In addition, open cell foams with large surface area-to-volume ratios have exhibited superior performance in enhancing heat transfer efficiency.

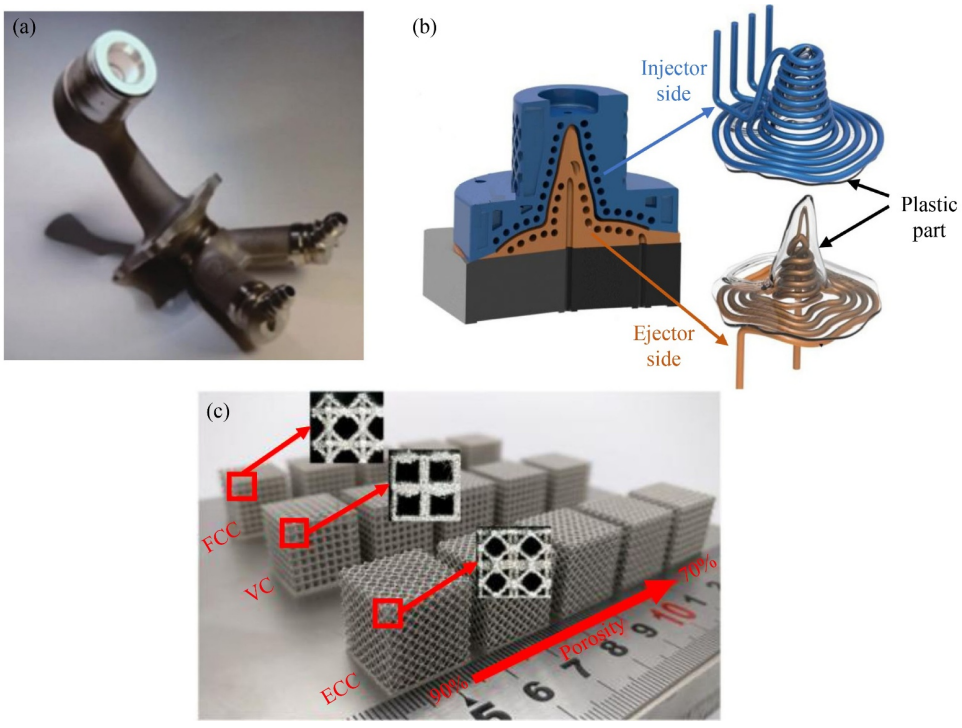

Fig. 4 Part images: (a) fuel nozzle with internal channel from the General Electric Company [66], (b) ejector side (orange) and injector side (blue) of mold with incorporated conformal cooling channels near to cavity [67], and (c) as built face center cube, vertex cube, and edge center cube structures [68] that prepared by laser-based powder bed fusion. Reproduced with permission from Ref. [68] from Elsevier.

Ho et al. [41] researched the heat transfer performance of different types of L-PBF lattice structures and proposed Rhombi-Octet lattice structure to improve single-phase forced convection cooling. Moreover, Jafari and Wits [65] reviewed the application of L-PBF technology on heat transfer devices and summarized the successful cell structures. In comparison with basic forms of internal structures, the combinations of different forms have also been designed and fabricated by L-PBF for practical applications (Fig. 5) [74].

Although the working principle of L-PBF provides excellent flexibility for the manufacture of various internal structures, applying L-PBF interior structures to specific applications has certain limitations, such as high internal surface roughness, low dimensional accuracy, and shape distortion given that L-PBF is an asymmetric fabrication method that depends on print direction. In addition, limited studies and inaccurate prediction of the overall performance of L-PBF internal structures have resulted in the lack of acceptance of this technology [75].

3 Surfaces of L-PBF internal structures

Given that surface quality has significant influence on various properties of products in practical applications [76–78], the causes of poor surface quality and the characteristics of surface features on L-PBF parts must be learned to facilitate the surface improvement of its products. Notably, L-PBF outer and internal surfaces are formed on the basis of the same mechanism and are affected by various effects, such as staircase effect and balling [16]. As a result, the outer and internal surfaces of L-PBF parts have similar surface features. To analyze the surface quality of L-PBF internal structures systematically, the combination of different types of surfaces and the complexity of specific internal structures should be considered.

3.1 Mechanism of causing poor surface quality

The behavior of molten pool and deposition angles are related to the final surface quality of L-PBF parts. As illustrated in Fig. 6 [79], L-PBF surfaces can be categorized into horizontal (top), up-facing (face up), vertical (side), and down-facing (face down) surfaces [79] according to different printing orientations. Due to the interaction of powder bed and laser, raw powders on the powder bed would be attracted by molten pools during the L-PBF process because of surface tension, hence resulting in adhered powders on the surface. After laser scanning, molten pools also solidify rapidly and leave uneven sintering tracks on the L-PBF surface. Generally, the temperature gradient mechanism is used to explain the unevenness of molten pools considering the property of previously solidified layers and the top layer being processed. Due to the rapid heating of the top layer by the laser beam and its low heat conductivity, a steep

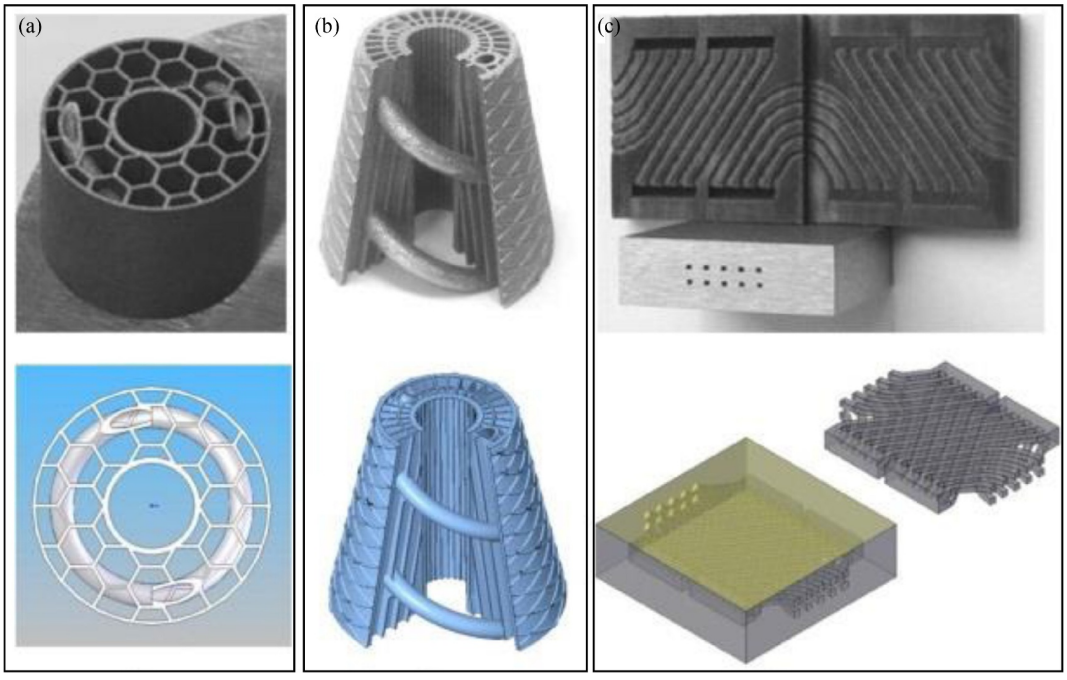

Fig. 5 Laser-based powder bed fusion parts (top) and their computer-aided design models (bottom) combined with different forms of internal structures: (a) cylinder with honeycomb inner structure and two spiral channels from 316L stainless steel, (b) conical frustum object with ribs and one spiral inner channel from 904L stainless steel, and (c) heat exchanger with complex cooling channels from Inconel 625 [74]. Reprinted with permission from Ref. [74] from Elsevier.

temperature gradient develops between the melt and solidified part. As the free expansion of the molten pool is restricted by surrounding materials, the top layer would bend away from the laser beam. Nevertheless, the compressed upper layers become shorter and form a bending angle toward the laser beam during the rapid solidification [80], as illustrated in Fig. 7 [23]. Thus, the topography of the molten pools on top surfaces is usually uneven. Furthermore, the irregular shape of the liquid molten pool is retained on the side, face up, and face down surfaces after solidification.

Notably, the staircase effect is more pronounced on face down surfaces than in other surfaces, as shown in Fig. 8 [15,16]. Strano et al. [15] studied L-PBF surface morphology and indicated that staircase effect was obvious at intervals of approximately 230 μm in Fig. 8(a) [15] on a 5° inclined surface. Cabanettes et al. [16] built samples with different inclinations and showed the visible staircase on an inclined surface in Fig. 8(b) [16]. Despite the optimization of layer thickness and although the sloping angle can weaken staircase effect, these parameters are generally constrained by many other factors, such as building orientation, residual stresses, CAD design, and production rate. Thus, changing these parameters directly to reduce the impact of staircase effect is difficult.

Balling effect refers to the spheroidization phenomena of molten pool caused by the instability of melts during the L-PBF process. The occurrence of balling is related to Plateau–Rayleigh instability and Marangoni convection [22]. During the first laser scanning, the powder bed can absorb energy from the laser beam and form a thermal gradient between the molten material and the surrounding powders. Then, the powder bed with a relatively low temperature tends to cause the melt to break up into metallic agglomerates with spherical shape to reduce surface energy. The balling phenomenon could increase surface roughness by forming surface protrusions, which may cause discontinuous or coarse laser scanning tracks [81]. In addition, pores are easily formed between discontinuous metallic balls, thereby resulting in the poor mechanical properties of L-PBF parts. Severer balling may cause the failure of powder spreading step when the paving roller is scratched by the rough surface [15,82].

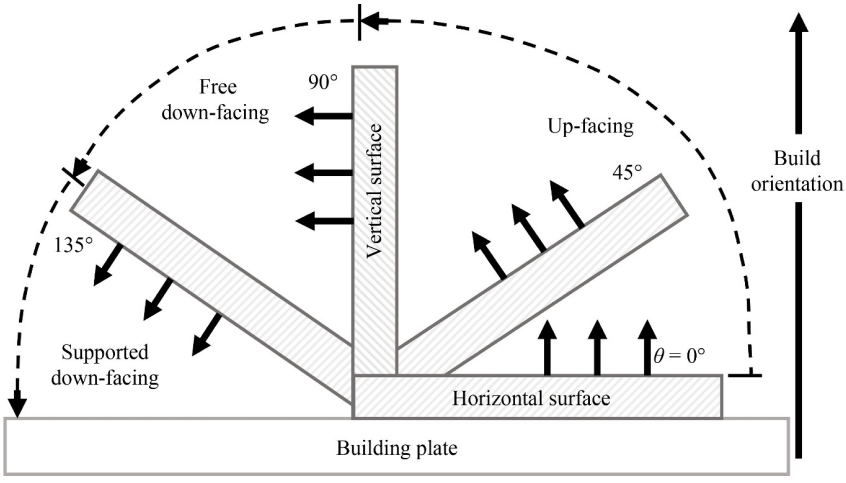

Fig. 6 Schematic of the different types of laser-based powder bed fusion surfaces according to their printing orientations [79]. Reproduced with permission from Ref. [79] from Elsevier.

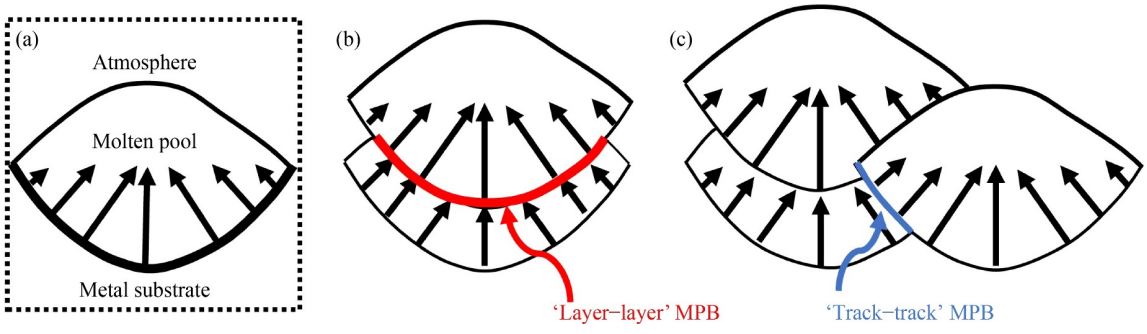

Fig. 7 Schematic of the crystallization solidification of molten pools during laser-based powder bed fusion process: (a) single molten pool, (b) "layer–layer" molten pool boundaries (MPB), and (c) "track–track" MPB. The arrows represent the grain orientations [23]. Reproduced with permission from Ref. [23] from Elsevier.

Balling effect can be influenced by many factors, such as laser scanning speed, oxygen content, laser power, and powder characteristics [82,83]. The oxygen content and wetting ability between the melt and the pre-processed layer is crucial for a successful deposition process. In fact, the oxide on the surface of the melts and sintered layers could impede the wettability of powders and cause balling because contamination layers could attribute to the radially inward Marangoni flow at higher dissolved oxygen contents [7,22]. Therefore, conducting L-PBF process in a protective atmosphere with inert gases is mandatory. In terms of laser scanning speed, discontinuous sintering tracks and balling could be formed under low energy input and poor wetting ability with higher scanning speed [82]. The effect of oxygen content is indicated in Fig. 9 [82], where an increase in oxygen content aggravated the size and degree of balling.

Surface defects, such as cracks and pores [84], can also occur if the fusion during the L-PBF is not controlled well. A good combination of L-PBF parameters and inert atmosphere are helpful in avoiding defects on the L-PBF surfaces. In addition, the influences of edge effect, gravity, overhanging surfaces, and heat transfer on surface quality also need to be considered.

3.2 Surface features

Based on the working principle of L-PBF, spherical protrusions and sintering tracks are evident morphologies on various L-PBF surfaces. Due to the spherical shape of raw powders, the spherical protrusions on the L-PBF surface were normally referred to as adhered powders. However, identifying the sintering degree of a powder by simply observing its spherical morphology is impossible. In practice, microstructure and property differences must be considered to identify L-PBF surface features.

The characterization of L-PBF surfaces considering the differences in microstructure and property has been paid attention to and carried out by researchers. Figure 10 [85] shows the surface microstructure of L-PBF AlSi7Mg (Fig. 10(a)) and cross-section on side surface (Fig. 10(b)). Notably, the adhered powder showed a microstructure transition from the raw powder to the sintered area throughout the spherical morphology, as can be seen in Fig. 10(c) [85]. Shen et al. [86] reported the microstructure differences of un-sintered powders and sintered area on top, face up, side, and face down surfaces of L-PBF 316L stainless steel. As shown in Figs. 11 [86] and 12 [86], the irregular shape of the solidified molten pools was retained on surfaces with different printing inclinations. Except for the sintered zone left by molten pools, the spherical morphologies on surfaces were characterized as un-sintered powders and sintered area. In terms of property, Nasab et al. [85] carried out the nano hardness profiles of a partially melted powder, and a transition zone between un-sintered powder and sintered

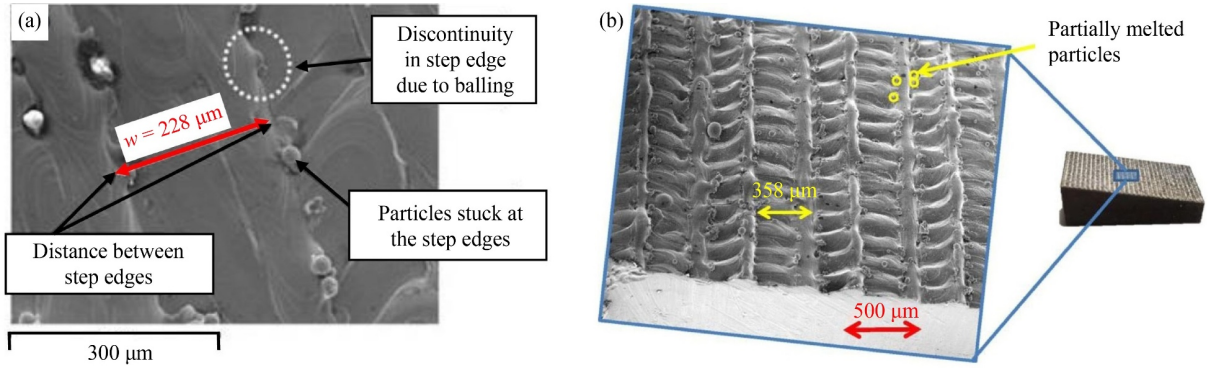

Fig. 8 Scanning electron microcopy images of (a) 5° inclined surface [15] and (b) an inclined sample with staircase effect clearly visible [16]. Reproduced with permissions from Refs. [15,16] from Elsevier.

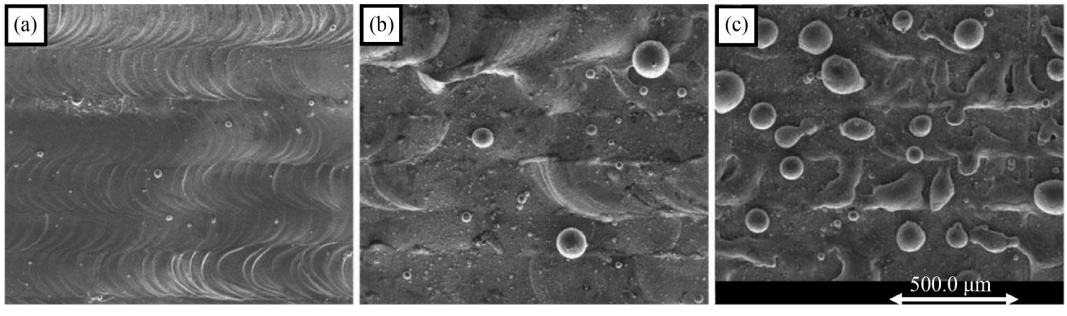

Fig. 9 Scanning electron microcopy images of balling characteristics with different oxygen contents during laser-based powder bed fusion: (a) 0.1%, (b) 2%, and (c) 10% [82]. Reproduced with permission from Ref. [82] from Springer Nature.

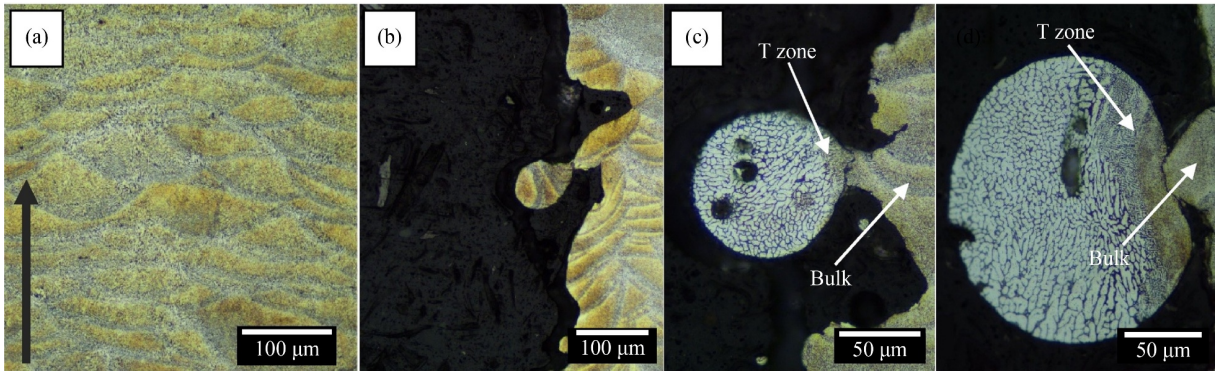

Fig. 10 Optical images of cross-sectional [85]: (a) bulk AlSi7Mg microstructure, (b) balling on the surface, and (c) partially melted spatters with spherical morphology on the surface. The arrow in (a) shows the build direction. Reproduced with permission from Ref. [85] from Elsevier.

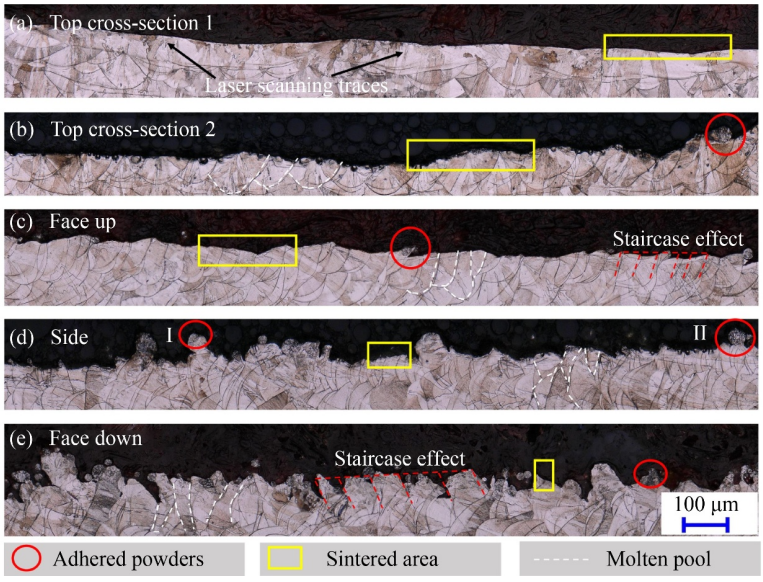

Fig. 11 Morphologies of etched cross-sections on raw laser-based powder bed fusion [86]: (a) top cross-section 1, (b) top cross-section 2, (c) face up, (d) side, and (e) face down surfaces.

area was proposed according to the changes in hardness values.

Given that the complexity of L-PBF surfaces and the characterization of surface features would affect surface evaluation and surface finish significantly studying the morphology, microstructure, property, and location of surface features in detail is therefore necessary and essential. Moreover, the bonding state and strength of un-sintered powders on L-PBF surface may vary on different types of surfaces because of the complicated solidification process. Thus, the sintering degree and bonding conditions of surface features should be characterized and identified precisely for further analysis.

3.3 Surface analysis of internal structures

The surface quality of L-PBF parts varies on different types of surfaces. The roughness of L-PBF surfaces is affected by building angles (Fig. 13 [87]), materials, and printing parameters. Moreover, it is a widely held view that the area ratios of sintered area and un-sintered powders vary on the top, face up, side, and face down surfaces considering the effects of staircase, heat conduction, gravity, and overhang. Bai et al. [88] applied L-PBF to fabricate the top and side surfaces of a 316L stainless steel and found that top surfaces had less adhered powders than side surfaces. Pakkanen et al. [47] studied the internal channel surface roughness and concluded that the surface roughness of L-PBF internal channels depended on their printing angles. Compared with other surfaces, the sintered area of face down surfaces usually possesses the highest roughness because heat conduction and gravity play more influential roles for overhanging these surfaces [16,87].

Considering that different printing angles are usually included in L-PBF internal structures and the L-PBF

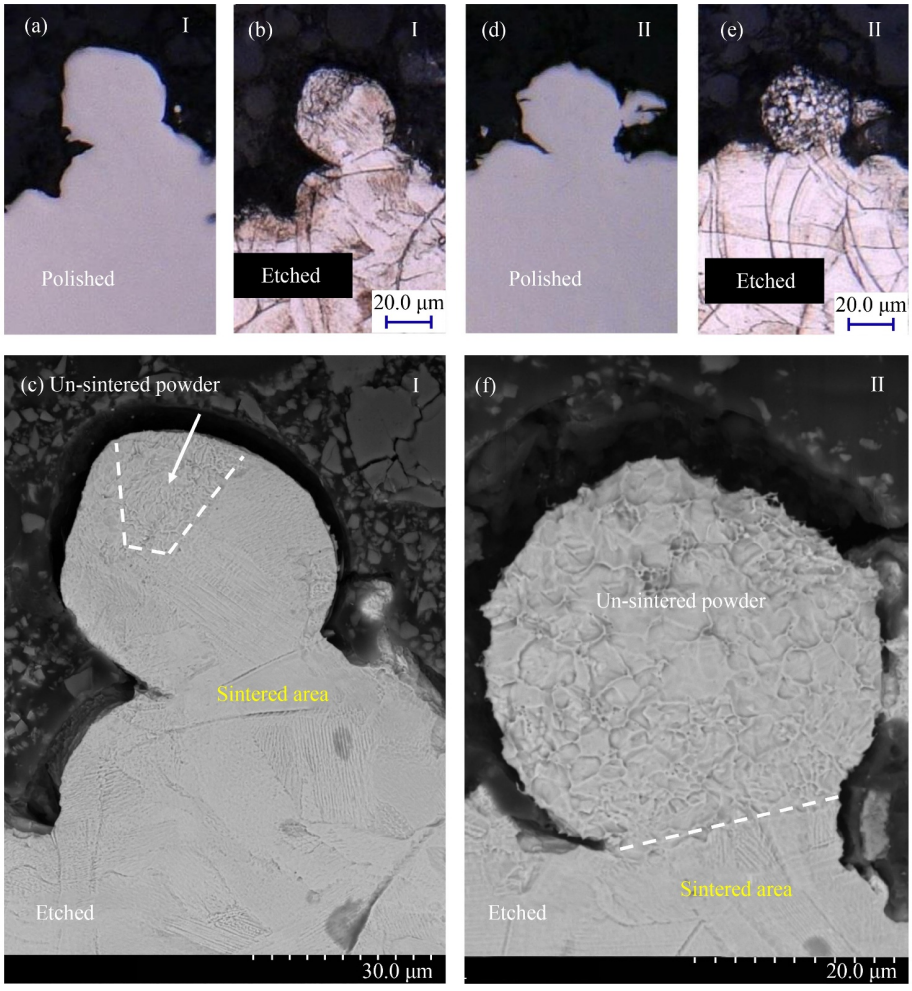

Fig. 12 Morphologies of (a) polished, (b) etched cross-section, (c) high magnification of etched cross-section at position I; (d) polished, (e) etched cross-section, and (f) high magnification of etched cross-section at position II in Fig. 11(d) [86].

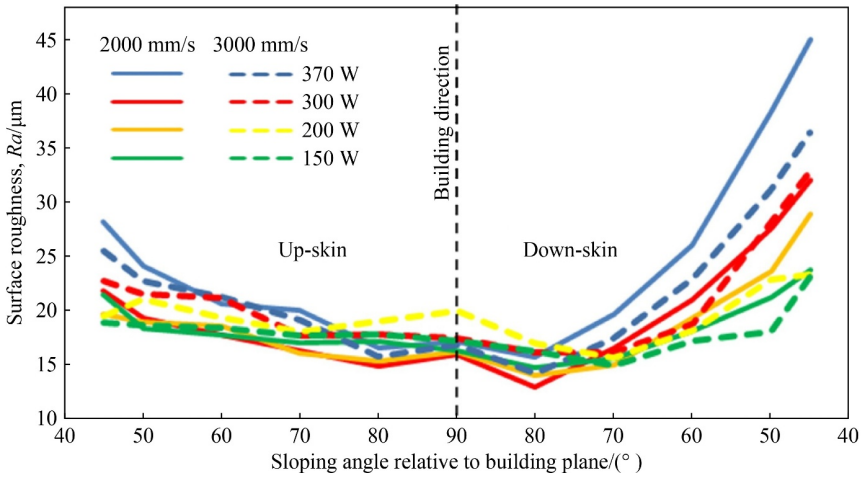

Fig. 13 Data graphs of face up and face down surface roughness of laser-based powder bed fusion Hastelloy X samples with different printing inclinations (45° to 90°) [87]. Reproduced with permission from Ref. [87] from Elsevier.

surface quality is affected by various effects and printing angles, the types of surfaces on the internal structures must also be identified. Figure 14 [71,89] presents two types of surfaces on the cross-section of a straight channel in Fig. 14(a) [71]. In terms of cellular structures, face up and face down surfaces are observed on the unit

cell of a body-centered cubic (BCC) lattice structure in Fig. 14(b). Furthermore, on the top view of the BCC lattice structure in Fig. 14(c) [89], the morphology of the top surface is characterized at the connection points of the struts. Thus, the L-PBF components with internal structures in Fig. 5 [74] contain different types of surfaces, and the internal surfaces must be analyzed according to the specific structure.

Given that the poor surface quality of L-PBF parts hinders the engineering applications, appropriate post treatments are required to improve surface quality for L-PBF parts, especially for L-PBF components with internal structures [87]. In addition, the complexity of L-PBF internal surfaces and structures make it challenging for post processing.

4 Polishing of L-PBF internal structures

The inferior surface quality of L-PBF components with internal structures is an obstacle in applying this technique to real industry production [90]. Considering that surface quality is critical for meeting specifications and tolerances, researchers have studied different approaches to improve the interior surface quality of L-PBF parts [91,92]. The typical approach is to optimize the fabrication strategy, which includes the design of raw powders [93], the optimization of L-PBF parameters [94–98], and the use of laser re-melting during L-PBF and others, such as the control of oxygen content in the atmosphere [99]. Although the optimized fabrication strategy is helpful in reducing balling and other surface defects, the adhesion of partially melted powders and rough sintered area are difficult to avoid completely. Another approach is the development of a hybrid process, in which L-PBF and a subtractive process, such as milling, are integrated to fabricate parts layer by layer [100–102]. Combining L-PBF and subtractive machining into one process is costly and limited to a few materials because the distortion issues of components can easily occur because of the absence of stress relief procedures during hybrid processing. Compared with fabrication optimization and hybrid processing technique, surface polishing methods based on material removal mechanisms are more economic and efficient for removing adhered powders and smoothening sintered area. Unlike L-PBF outer surfaces that could use various methods, such as blasting and laser polishing for surface improvement [103], it is in high demand and more challenging to polish interior surfaces on L-PBF parts. In recent years, researchers have developed different polishing techniques for L-PBF internal structures. The existing polishing methods for L-PBF internal structures can be categorized to three aspects, namely, mechanical, chemical, and hybrid methods, according to mechanisms [104,105].

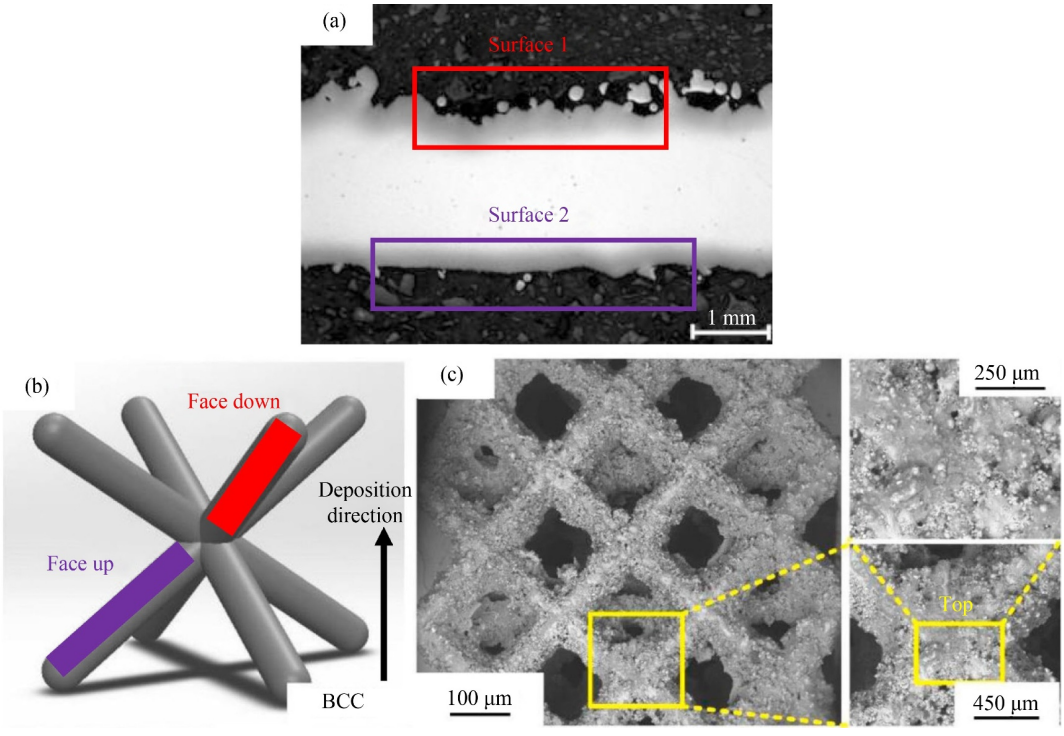

Fig. 14 Different types of surfaces of (a) a laser-based powder bed fusion straight channel with its cross-sectional optical micrograph [71], (b) a unit cell of BCC lattice structure, and (c) the top view of the laser-based powder bed fusion BCC lattice structures [89]. BCC: body-centered cubic. Reproduced with permission from Ref. [71] from Elsevier.

4.1 Mechanical methods

Mechanical polishing methods generally utilize power-driven abrasive media as cutting tools to smooth L-PBF interior surfaces. Nowadays, AFM, magnetic abrasive finishing (MAF), AFP, and barrel finishing (BF) have been applied to complete surface finish of L-PBF parts with internal structures. Although there are some common features, such as the independence of raw surface quality among these mechanical polishing processes, each technology has its specific polishing characteristics and is suitable for different types of interior structures. The working principles of some mechanical polishing methods are shown in Fig. 15 [106,107].

AFM corresponds to a machining process that can be used to deburr, polish, and remove recast layer. By using two vertically opposed cylinders, the surface material on the fixed workpiece can be removed when the pressurized semi-solid laid with hard abrasive particles repeatedly flows through a restricted passageway, as shown in Fig. 15(a) [106]. Based on the working principles of AFM, it is considered for finishing components with complex geometries and internal structures. The use of AFM parameters, such as extrusion pressure, number of cycles, and media composition, need to be considered for parts with different hardness, geometries, and initial surface qualities [108]. Nowadays, AFM has been widely used for the polishing of L-PBF straight and curve channels. Han et al. [1,109] applied AFM to L-PBF conformal cooling channels in mold industry and indicated that AFM was more efficient in removing protruding features than valleys on L-PBF surface [1]. In terms of the residual stress and fatigue performance, AFM was capable of improving the fatigue resistance of L-PBF channel by increasing its compressive stress [109]. Apart from experiments, Ferchow et al. [110] proposed a pressure–velocity-based model to simulate the roughness and thickness reduction quantitatively during AFM for L-PBF curve channels. Nevertheless, expanding AFM to thin wall channels or cellular structures is difficult because the use of high pressure easily damages these structures. Moreover, the viscous media with high pressure in AFM may remain or embed into L-PBF surface and cause contamination. Furthermore, achieving uniform material removal on L-PBF channels with varied geometries is difficult for AFM to achieve.

MAF [107] applies magnetic abrasive particles to grind workpiece surface. For L-PBF straight channels, the magnetic abrasive media is generally pressed against the surface by magnetic force. Meanwhile, the rotation of workpiece and linear vibration of magnets induce relative motion between the abrasive particles and the sample surface, as can be seen in Fig. 15(b) [107]. Thus, the abrasive particles acted as a flexible magnetic abrasive brush and dragged along the internal surfaces to remove materials. Guo et al. [107] investigated the MAF process on a straight tube that was prepared by L-PBF Inconel 718 alloy. Polishing results indicated that MAF could remove partially melted powders efficiently and decrease the surface roughness *Ra* from 7 to less than 1 μm. Although MAF is a promising polishing method for L-PBF internal structures, its drawback lies in its limitation on suitable materials for processing. For example, the polishing effect of MAF is negligible on ferromagnetic material, such as nickel and cobalt alloys. Furthermore, MAF is more suitable for polishing internal features with rotational symmetry rather than complicated features and protrusions because magnetic abrasive particles cannot navigate around these internal features [111].

AFP is a finishing process performed by combining liquid impingement and abrasion from abrasive particles. In the AFP process, the surface is polished when the fluid with free abrasive grains passes through the workpiece. AFP can polish surfaces with various initial conditions because of its working mechanism. Due to the mechanical removal mechanism, AFP could also be applied in various L-PBF materials. Compared with traditional AFM, which uses high pressure and an abrasive laden media as tool, a lower pumping pressure and viscosity

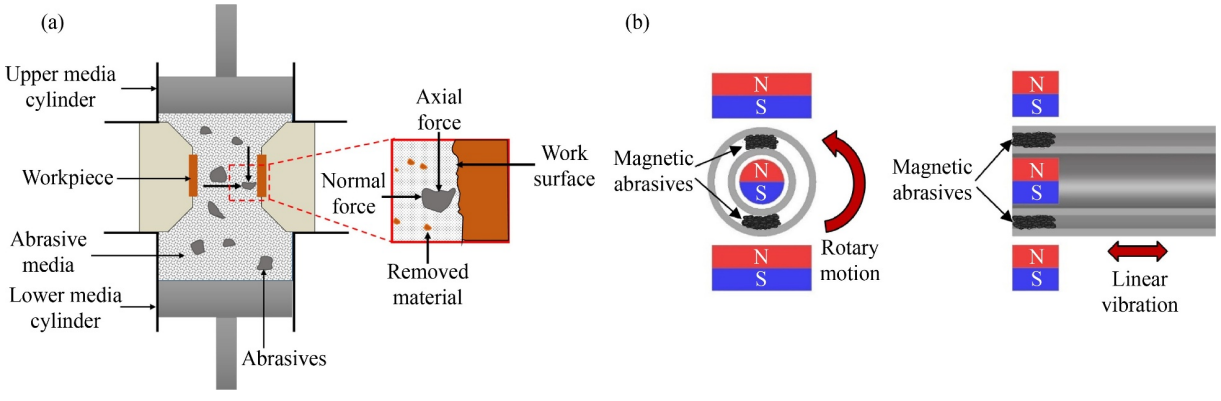

Fig. 15 Schematic of (a) abrasive flow machining [106] and (b) magnetic abrasive finishing [107]. Reproduced with permissions from Refs. [106,107] from Elsevier.

fluid, as well as a higher flow velocity, are utilized in AFP [112]. Moreover, unlike limitations, such as contamination and abrasive agglomeration in AFM, AFP is more suitable for polishing thin-walled and lattice structures without damage and contamination [12]. Thus, AFP is preferred for polishing L-PBF parts with various internal structures in aerospace and mold industries [113]. To improve the poor surface quality of L-PBF parts, researchers investigated the material removal mechanism and various parameters of AFP in the polishing of L-PBF internal structures. Furumoto et al. [8] developed an AFP apparatus and found that the efficiency of AFP decreased with the increase in polishing time. Nagalingam et al. [12] investigated liquid impingement and absolute abrasion. They found that liquid impingement and particle abrasion were effective in removing loose powders and partially melted particles on L-PBF straight channels. The limitations of AFP, for instance, the long polishing time and low processing efficiency, come from the use of low pressure and solution viscosity. Besides, the performance of AFP depends on the hardness and wear property of materials. Thus, AFP is often applied to alloys with low hardness, such as AlSi10Mg.

BF, also known as tumble finishing, generally reduce surface roughness by the mechanical rotation of a barrel that contains a mixture of samples and grinding media [103]. Because no part fixing is required, various materials with L-PBF complex geometries can be processed [14]. Boschetto et al. [114] applied ceramic media with different sizes in BF and found that the prominent reduction of surface roughness was achieved after 20 h of BF on an L-PBF Ti–6Al–4V impeller. Khorasani et al. [115] investigated the effects of various BF parameters and confirmed that the roughness of L-PBF various surfaces declined by more than 50% after wet abrasive centrifugal BF process. Compared with AFM, MAF, and AFP, BF is more applicable to structures with large internal size because the media in BF usually have a millimeter scale. In addition, BF needs hours of polishing to reduce surface roughness, which means the polishing efficiency of BF is lower than those of other mechanical methods.

4.2 Chemical-based methods

Chemical treatment is mainly based on chemical reactions that occur at the interface between surface and reactive chemicals. Benefiting from the fluidity of the solution, the polishing media of chemical polishing (CP) and EP can contact with the inner surface, hence making them suitable candidates for the surface improvement of L-PBF internal structures [116].

In the CP process, the uneven areas on metal or alloy surfaces are dissolved selectively by chemical etching to achieve leveling effect. The equipment of CP is simple and is capable of dealing with channels, cellular structures, or combined complex internal structures. CP could reduce the peak-to-valley spacing on L-PBF Ti–6Al–4V surface and form a passivation film for the improvement of surface corrosion resistance in the meantime [117]. Generally, the CP process for L-PBF titanium alloys utilizes etchants with hydrofluoric acid and nitric acid. Lyczkowska et al. [116] used CP to improve the surface quality of L-PBF Ti–6Al–7Nb components with lattice structure. The removal of adhered powders and reduction of surface roughness were influenced mostly by chemical composition and concentration. Despite the effectiveness of the process, CP tends to erode material indiscriminately, hence compromising the dimensional accuracy of L-PBF components [118]. Although the addition of strong acid with high concentration to chemical etchants could accelerate chemical reactions, it is harmful to the environment and may influence the performance of medical products after CP [117,118].

EP is a finishing process for metals or alloys to achieve smooth and bright surfaces based on anodic dissolution. During EP, the material is dissolved ion by ion from a workpiece due to the combination of electricity and chemical reaction. Final EP results are influenced by many factors, such as current density, temperature, electrolyte type, and initial surface roughness [119]. In general, EP is composed of anodic levelling (macro-smoothening) and brightening (micro-smoothening) [120]. Moreover, the surface quality of a part is improved after EP because of the removal of the original layer and the formation of a new, homogenous oxide film. Different from traditional mechanical finishing techniques, such as milling or grinding, EP is a non-contact and damage-free process. Moreover, EP also has characteristics, such as simplicity of device, flowability of electrolyte, designability of cathode tool, and high material removal rate, thereby making it suitable to polish L-PBF channels and cellular structures [121]. Chang et al. [9] proposed a combination of overpotential and conventional EP processes to remove adhered powders and smooth the struts on L-PBF 316L stainless steel lattice structures. Dong et al. [122] also investigated the effect of EP parameters on L-PBF Ti–6Al–4V lattice structures via Taguchi method. Evidently, EP can polish L-PBF internal surfaces, particularly, it can remove partially melted powders and smoothen laser sintered tracks, as shown in Fig. 16 [123]. The effects of EP on various L-PBF alloys (e.g., Ti-based alloys [79], Al-based alloys [9], nickel-based alloys [90], Fe-based alloys [9], and Co–Cr alloys [124]) have also been studied in recent years.

Despite the advantages and wide applications of EP, the use of this technology in the post-treatment of L-PBF internal structures also have limitations and challenges. Considering that the surface roughness of L-PBF components usually varies from 10–20 μm in *Ra* [125], the rough initial surface will impede a fast and effective

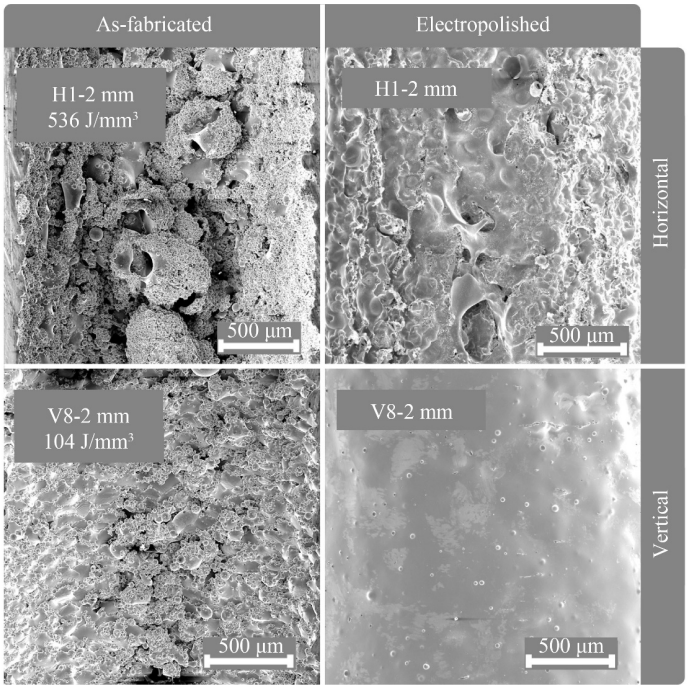

Fig. 16 Scanning electron microcopy images of interior channel morphology before and after electropolishing of horizontal channel and vertical channel walls [123]. Reproduced with permission from Ref. [123] from Elsevier.

EP process [120]. In terms of L-PBF internal structures with high complexity, EP experiences difficulty in achieving a uniform surface finish because of the limited accessibility of cathode tool [12]. Moreover, no available theory explains EP mechanisms well because of the complexity of current, chemical reactions, ion transport, and diffusion at workpiece-electrolyte interface [120]. In addition, environmentally friendly electrolytes, which also consider EP efficiency, are expected because of safety concerns. Thus, the in-depth study of EP and development of innovative technologies based on EP are strongly necessary to benefit from the production process of L-PBF.

4.3 Hybrid methods

Hybrid polishing technologies are generally developed on the basis of various single polishing processes to overcome the weakness of one method or improve its polishing performance. Notably, the hybrid methods presented in this section refer to combining different polishing processes into one polishing procedure. Current hybrid polishing technologies are classified into AFP-based and EP-based hybrid polishing processes for L-PBF internal structures.

Recently, researchers developed various hybrid polishing processes based on AFP to improve its polishing efficiency [12]. Mohammadian et al. [10] combined AFP and CP for the interior surface of L-PBF Inconel 625 alloy. In polishing experiments, chemical abrasive fluid is mixed and then pumped to pass through the sample chamber to finish the polishing process. Surface roughness data showed that chemical flow polishing resulted in a higher reduction of surface roughness compared with single CP process. Although the efficiency of hybrid polishing is improved, it has limitations similar to those of CP, such as the use of strong acid. Unlike the use of hazard chemicals to facilitate polishing efficiency, Nagalingam et al. [12] applied hydrodynamic cavitation in AFP and proposed hydrodynamic cavitation abrasive finishing (HCAF) technique for L-PBF straight channels. Figure 17 [12] displays that a cavitation inducer is placed upstream at the inlet of the HCAF chamber to induce a hydrodynamic cavitation stream in the fluid flow. The investigation indicated that the synergistic effects showed higher material removal rate on L-PBF straight channels than single cavitation and abrasion process. Although the development of AFP-based hybrid polishing methods exhibit higher polishing efficiency for channels, the mechanism and controllability of hybrid polishing based on AFP are more complicated and worthy of further study.

EP-based hybrid polishing techniques for various L-PBF internal structures are attractive because they possess the advantages of EP, such as high material removal rate. Zhao et al. [11] proposed an electrochemical mechanical polishing (ECMP) process for L-PBF internal holes by using a metallic wire as cathode and nylon filaments as flexible abrasive. During ECMP, the electrochemical reaction takes place while nylon filaments that are fixed on the cathode could scratch the

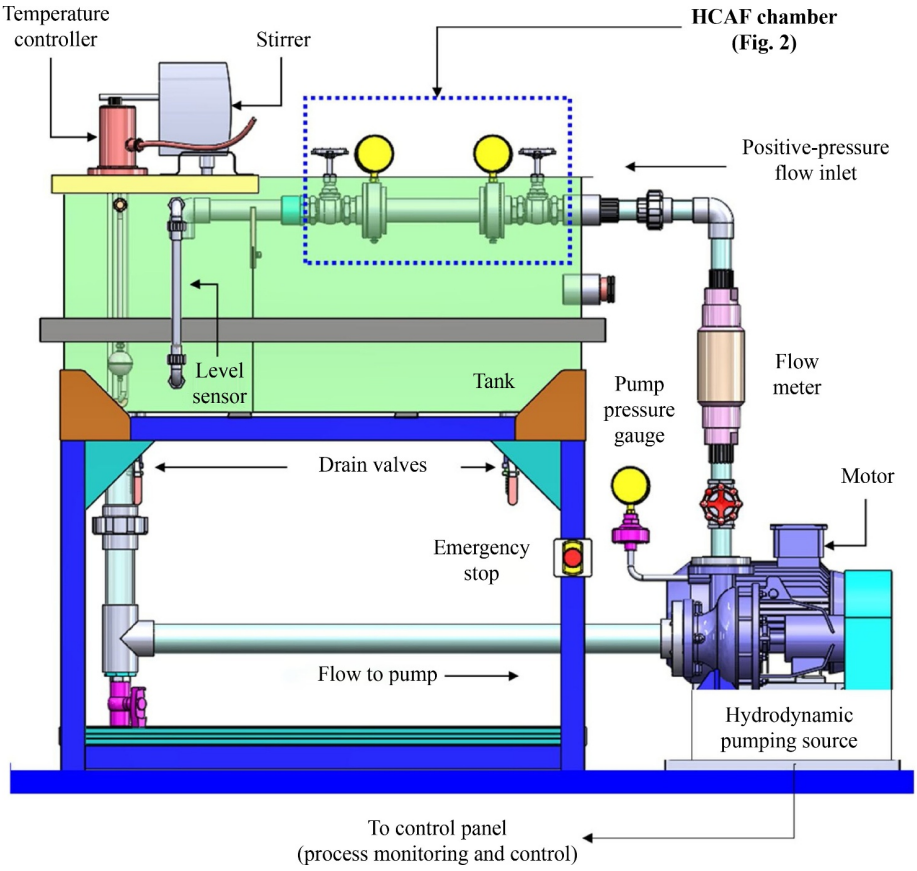

Fig. 17 Schematic of HCAF apparatus [12]. HCAF: hydrodynamic cavitation abrasive finishing. Reproduced with permission from Ref. [12] from Elsevier.

internal surface mechanically following the movement of the wire. However, extending this technique to complex curve channels or lattice structures is difficult because of the use of nylon filaments and rigid metallic wire. In addition, the polishing effect and mechanism of dry mechanical-electrochemical polishing [88] was also studied, but the smallest internal features that can be polished are limited to the size of the dry electrolyte media particles.

4.4 Comparison of various methods

Based on the mechanism difference, various polishing methods have their own polishing characteristics for L-PBF internal structures. To compare the polishing effect and efficiency of polishing methods, the materials, polishing time, and surface roughness of L-PBF internal structures before and after polishing are summarized in Table 2 [1,8,9,11,107,127,128]. In general, EP and EP-based hybrid polishing methods have higher material removal rate than other methods due to the use of electricity. In terms of internal structures, EP-based methods are more suitable in facilitating the placement of cathodes. Due to the use of high pressure, AFM is more suitable for polishing L-PBF complex channels with a certain wall thickness, whereas AFP-based methods could be used to polish lattice structures and thin-walled channels. In addition, the properties of the polishing medium also affect the suitability of polishing techniques. CP-based methods have been applied to polish various internal structures because of the high fluidity and low viscosity of the polishing solution. Compared with CP- and EP-based polishing methods, AFP, MAF, and BF could be applied to internal structures with different internal dimensions considering the size of the abrasive particles.

Due to the material removal process, the use of various polishing methods could alter the topography of L-PBF inner surfaces. Moreover, some polishing methods may also affect the shape and size of internal structures, as illustrated in Fig. 18 [9,110,128]. Ferchow et al. [110] prepared straight channels with face up and face down surfaces by L-PBF and measured the diameter and roughness of the channel at different positions before and after AFM. Figure 18(a) [110] illustrates that the removed thickness changed at different positions of the channel after AFM. The material removal rate at the inlet or entrance of the channel was higher than that at the intermediate region during AFM. As a result, the diameter of the two ends of the channel increased.

Table 2 List of polishing methods, materials, polishing time, and surface roughness before and after the polishing of L-PBF internal structures [1,8,9,11,107,127,128]

Polishing method	Material	Internal structure	Raw surface roughness/μm	Polishing time/min	Polished surface roughness/μm
AFM [1]	Maraging steel 300	Φ 3 mm curve channel	*Sa* = 9.70	≈ 80.00	*Sa* = 3.30
MAF [107]	Inconel 718	Φ 24 mm straight channel	*Ra* = 7.22	180.00	*Ra* = 0.23
AFP [8]	Alloy	Φ 5 mm straight channel	*Rz* ≈ 110.00	133.00	*Rz* ≈ 20.00
CP [127]	316L stainless steel	Straight channel	*Sa* = 13.80	45.00	*Sa* = 5.22
EP [9]	316L stainless steel	Lattice structure	*Ra* ≈ 8.00	40.00	*Ra* ≈ 0.18
HCAF [128]	AlSi10Mg	5 mm × 5 mm straight channel with square cross-section	*Ra* ≈ 18.00	180.00	*Ra* ≈ 4.00
ECMP [11]	304 stainless steel	Φ 10 mm straight channel	*Sa* = 14.51	2.86	*Sa* = 9.09

Notes: *Ra*: arithmetical mean deviation of line, *Sa*: arithmetical mean deviation of surface area, *Rz*: average of the vertical distances from the highest peak to the lowest valley.

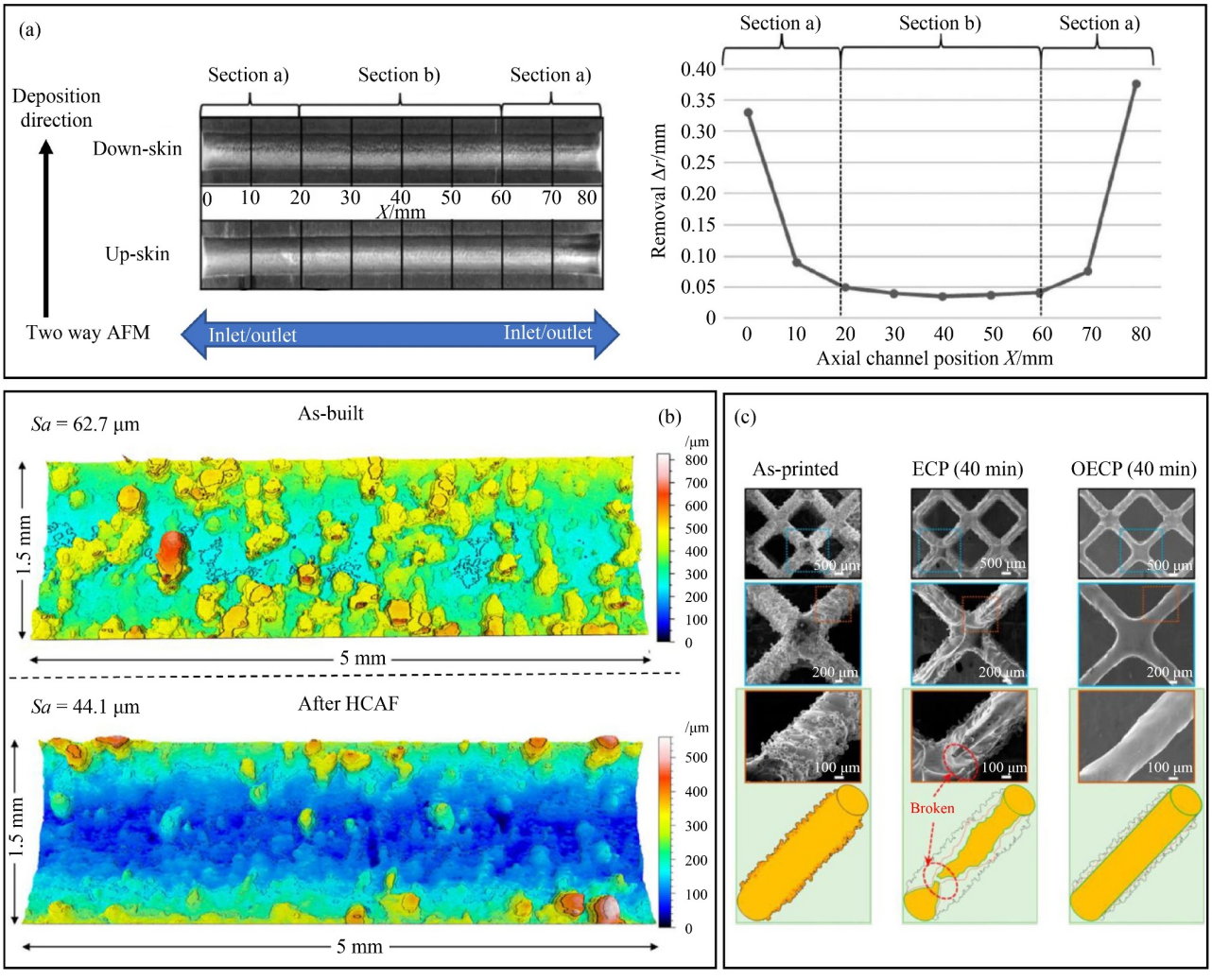

Fig. 18 Part images of (a) quantitative results showing diameter removal differences at different positions of a laser-based powder bed fusion channel after two-way AFM [110], (b) surface topography of laser-based powder bed fusion channel before and after HCAF process [128], and (c) morphology comparison of laser-based powder bed fusion body-centered cubic lattice structures before and after electrochemical polishing (ECP) and overpotential electrochemical polishing (OECP) [9]. AFM: abrasive flow machining, HCAF: hydrodynamic cavitation abrasive finishing. Reproduced with permissions from Refs. [110,128] from Emerald Publishing Limited and Elsevier, respectively.

Compared with AFM, the polishing pressure during the HCAF process is much lower, and Fig. 18(b) [128] compared the internal surface topography of an L-PBF channel before and after HCAF. The results showed that

HCAF could remove adhered powders and reduce surface roughness effectively. Considering the high material removal rate, poor EP parameters may affect dimensional accuracy or even damage the internal structure with thin strut in Fig. 18(c) [9]. To accurately evaluate the effect of polishing on surface topography and dimension of L-PBF internal structures, the topography, roughness, and size of multiple identical locations must be measured before and after polishing.

To facilitate the productization of the internal structure of L-PBF, the medical industry generally adopts chemical methods. Moreover, almost all polishing methods can be used for various applications, such as AFP for conformal cooling channels in the mold industry. Considering the surface and structural complexity of L-PBF internal structures, current polishing methods were investigated for the polishing of simple or single-form internal structures. Thus, the polishing technologies for L-PBF internal structures still have a great room for development and improvement to expand their applications.

5 Conclusions and perspective

This study mainly serves as a review of the process, surface, and polishing methods for L-PBF internal structures. The internal structures on metallic parts are common for industrial use and academic study. However, the poor surface quality of L-PBF products limits their wide applications. Thus, various polishing methods have been developed for the inner surface finish of L-PBF components. The main conclusions can be drawn as follows.

1) Based on the use of a high-power laser and complete melting mechanism, raw powders experience rapid melting, form molten pools, and then solidify rapidly during L-PBF. Hence, this technology has been widely used to fabricate various materials. The layer-by-layer principle and rapid development of L-PBF have enabled it to prepare parts with complex internal structures. Channels and cellular structures are typical interior structures that have been used on L-PBF metallic parts because of their specific functionality. L-PBF components with various internal structures show great potential in practical applications. However, the inner structures of L-PBF still face challenges, especially the inferior surface quality for applications.

2) The poor surface quality of L-PBF products is influenced by the behavior of molten pool and various factors. In general, top, face up, side, and face down surfaces are observed for L-PBF part according to different printing angles. Based on the same deposition principle, similar surface features, such as un-sintered powders and sintered area, have been characterized on various L-PBF surfaces considering morphology, microstructure, and property differences. Due to the complexity of L-PBF surfaces and internal structures, the surface types and characteristic of the specific structure need to be investigated to analyze the surface quality of L-PBF internal structures accurately and comprehensively.

3) Mechanical, chemical, and hybrid polishing methods have been developed and utilized for the inner surface finish of L-PBF parts. Due to mechanism difference, each polishing technique is suitable for specific L-PBF internal structures. Meanwhile, the polishing effect and efficiency vary widely. In addition, the influences of surface finish techniques on the topography and dimension of L-PBF internal structures need to be considered. Although polishing is an effective and economical way for improving surfaces, the relationship between L-PBF surface features and their corresponding material removal mechanisms during polishing has not been established well.

From the perspective of polishing of L-PBF internal structures, future studies should focus on the following aspects:

1) To accelerate the industrial application of L-PBF internal structures, more efforts should be devoted to establishing the connection among the design, materials, deposition parameters, structure optimization, mechanical performance, surface properties, and polishing. Given that the polishing of L-PBF internal structures is generally performed from the raw surfaces, the characterization of L-PBF surface features and their bonding conditions requires a detailed study that considers differences, such as morphology, microstructure, and properties.

2) Although various polishing methods have been applied in practical applications, the material removal mechanism and main parameters of each method still have aspects that have not been studied clearly. Thus, comprehensive studies of surface characterization, polishing process, numerical simulations, and surface properties are essential considering their significant impact on the selection of an appropriate surface finish method for L-PBF internal structures. Considering the complexity of surface and geometry of L-PBF internal structures, breakthroughs and innovations in parameter investigation, fixture design, and optimization are required for current polishing methods to improve the accuracy of surface finish.

3) With the increasing demand from the industry, developing innovative polishing technologies with high efficiency is of great significance. In addition, the surface measurement and evaluation methods for L-PBF internal structures need further development. Compared with straight channel, conducting the surface roughness measurement, geometry measurement, and topography characterization of curve channels and lattice structures is inconvenient. Considering the importance of surface evaluation and the characteristics of specific internal structures, effective measurement methods are expected

to be developed to improve the accuracy and convenience of measurement.

Nomenclature

3D	Three-dimensional
AFM	Abrasive flow machining
AFP	Abrasive fluid polishing
AM	Additive manufacturing
BCC	Body-centered cubic
BF	Barrel finishing
CAD	Computer-aided design
CP	Chemical polishing
ECMP	Electrochemical mechanical polishing
EP	Electropolishing
HCAF	Hydrodynamic cavitation abrasive finishing
LAM	Laser additive manufacturing
LMD	Laser melting deposition
L-PBF	Laser-based powder bed fusion
LS	Laser sintering
MAF	Magnetic abrasive finishing

Acknowledgements This publication has emanated from research supported by the Science Foundation Ireland (Grant Nos. 16/RC/3872 and 15/RP/B3208). For the purpose of Open Access, the authors have applied a CC BY public copyright license to any Author Accepted Manuscript version arising from the submission. The authors would like to thank the "111" Project by the State Administration of Foreign Experts Affairs and the Ministry of Education of China (Grant No. B07014).

Funding note Open Access funding provided by the IReL Consortium.

References

1. Han S, Salvatore F, Rech J, Bajolet J. Abrasive flow machining (AFM) finishing of conformal cooling channels created by selective laser melting (SLM). Precision Engineering, 2020, 64: 20–33
2. Huo P Z, Zhao Z Y, Bai P K, Yuan X L, Wang Q, Zhao R X, Zhang L Z, Du W B, Han B, Wang Y. Deformation evolution and fracture mechanism of porous TC4 alloy scaffolds fabricated using selective laser melting under uniaxial compression. Journal of Alloys and Compounds, 2021, 861: 158529
3. Nakazawa K, Ozawa S, Iwata F. Additive manufacturing of metal micro-ring and tube by laser-assisted electrophoretic deposition with Laguerre–Gaussian beam. Nanomanufacturing and Metrology, 2021, 4(4): 271–277
4. Fang F Z, Zhang X D, Gao W, Guo Y B, Byrne G, Hansen H N. Nanomanufacturing—perspective and applications. CIRP Annals, 2017, 66(2): 683–705
5. Yan X C, Li Q, Yin S, Chen Z Y, Jenkins R, Chen C Y, Wang J, Ma W Y, Bolot R, Lupoi R, Ren Z M, Liao H L, Liu M. Mechanical and *in vitro* study of an isotropic Ti6Al4V lattice structure fabricated using selective laser melting. Journal of Alloys and Compounds, 2019, 782: 209–223
6. Yadroitsev I, Thivillon L, Bertrand P, Smurov I. Strategy of manufacturing components with designed internal structure by selective laser melting of metallic powder. Applied Surface Science, 2007, 254(4): 980–983
7. Gu D D, Meiners W, Wissenbach K, Poprawe R. Laser additive manufacturing of metallic components: materials, processes and mechanisms. International Materials Reviews, 2012, 57(3): 133–164
8. Furumoto T, Ueda T, Amino T, Hosokawa A. A study of internal face finishing of the cooling channel in injection mold with free abrasive grains. Journal of Materials Processing Technology, 2011, 211(11): 1742–1748
9. Chang S, Liu A H, Ong C Y A, Zhang L, Huang X L, Tan Y H, Zhao L P, Li L Q, Ding J. Highly effective smoothening of 3D-printed metal structures via overpotential electrochemical polishing. Materials Research Letters, 2019, 7(7): 282–289
10. Mohammadian N, Turenne S, Brailovski V. Surface finish control of additively-manufactured Inconel 625 components using combined chemical-abrasive flow polishing. Journal of Materials Processing Technology, 2018, 252: 728–738
11. Zhao C H, Qu N S, Tang X C. Electrochemical mechanical polishing of internal holes created by selective laser melting. Journal of Manufacturing Processes, 2021, 64: 1544–1562
12. Nagalingam A P, Yuvaraj H K, Yeo S H. Synergistic effects in hydrodynamic cavitation abrasive finishing for internal surface-finish enhancement of additive-manufactured components. Additive Manufacturing, 2020, 33: 101110
13. Vayre B, Vignat F, Villeneuve F. Metallic additive manufacturing: state-of-the-art review and prospects. Mechanics & Industry, 2012, 13(2): 89–96
14. Boschetto A, Bottini L, Veniali F. Surface roughness and radiusing of Ti6Al4V selective laser melting-manufactured parts conditioned by barrel finishing. The International Journal of Advanced Manufacturing Technology, 2018, 94(5–8): 2773–2790
15. Strano G, Hao L, Everson R M, Evans K E. Surface roughness analysis, modelling and prediction in selective laser melting. Journal of Materials Processing Technology, 2013, 213(4): 589–597
16. Cabanettes F, Joubert A, Chardon G, Dumas V, Rech J, Grosjean

C, Dimkovski Z. Topography of as built surfaces generated in metal additive manufacturing: a multi scale analysis from form to roughness. Precision Engineering, 2018, 52: 249–265
17. Kasperovich G, Hausmann J. Improvement of fatigue resistance and ductility of TiAl6V4 processed by selective laser melting. Journal of Materials Processing Technology, 2015, 220: 202–214
18. Qiu C L, Panwisawas C, Ward M, Basoalto H C, Brooks J W, Attallah M M. On the role of melt flow into the surface structure and porosity development during selective laser melting. Acta Materialia, 2015, 96: 72–79
19. Sun Z J, Tan X P, Tor S B, Yeong W Y. Selective laser melting of stainless steel 316L with low porosity and high build rates. Materials & Design, 2016, 104: 197–204
20. Zhang L C, Attar H. Selective laser melting of titanium alloys and titanium matrix composites for biomedical applications: a review. Advanced Engineering Materials, 2016, 18(4): 463–475
21. Yadroitsev I, Gusarov A, Yadroitsava I, Smurov I. Single track formation in selective laser melting of metal powders. Journal of Materials Processing Technology, 2010, 210(12): 1624–1631
22. Rombouts M, Kruth J P, Froyen L, Mercelis P. Fundamentals of selective laser melting of alloyed steel powders. CIRP Annals, 2006, 55(1): 187–192
23. Wen S F, Li S, Wei Q S, Yan C Z, Zhang S, Shi Y S. Effect of molten pool boundaries on the mechanical properties of selective laser melting parts. Journal of Materials Processing Technology, 2014, 214(11): 2660–2667
24. Xu W, Brandt M, Sun S, Elambasseril J, Liu Q, Latham K, Xia K, Qian M. Additive manufacturing of strong and ductile Ti–6Al–4V by selective laser melting via *in situ* martensite decomposition. Acta Materialia, 2015, 85: 74–84
25. Qiu C L, Adkins N J E, Attallah M M. Microstructure and tensile properties of selectively laser-melted and of HIPed laser-melted Ti–6Al–4V. Materials Science and Engineering: A, 2013, 578: 230–239
26. Li R, Shi Y, Wang Z, Wang L, Liu J, Jiang W. Densification behavior of gas and water atomized 316L stainless steel powder during selective laser melting. Applied Surface Science, 2010, 256(13): 4350–4356
27. Ma M, Wang Z M, Gao M, Zeng X Y. Layer thickness dependence of performance in high-power selective laser melting of 1Cr18Ni9Ti stainless steel. Journal of Materials Processing Technology, 2015, 215: 142–150
28. Xin X Z, Chen J, Xiang N, Wei B. Surface properties and corrosion behavior of Co–Cr alloy fabricated with selective laser melting technique. Cell Biochemistry and Biophysics, 2013, 67(3): 983–990
29. Li Y, Gu D. Parametric analysis of thermal behavior during selective laser melting additive manufacturing of aluminum alloy powder. Materials & Design, 2014, 63: 856–867
30. Read N, Wang W, Essa K, Attallah M M. Selective laser melting of AlSi10Mg alloy: process optimisation and mechanical properties development. Materials & Design (1980–2015), 2015, 65: 417–424
31. Niu X D, Singh S, Garg A, Singh H, Panda B, Peng X B, Zhang Q J. Review of materials used in laser-aided additive manufacturing processes to produce metallic products. Frontiers of Mechanical Engineering, 2019, 14(3): 282–298
32. Harrison N J, Todd I, Mumtaz K. Reduction of micro-cracking in nickel superalloys processed by selective laser melting: a fundamental alloy design approach. Acta Materialia, 2015, 94: 59–68
33. Carter L N, Martin C, Withers P J, Attallah M M. The influence of the laser scan strategy on grain structure and cracking behaviour in SLM powder-bed fabricated nickel superalloy. Journal of Alloys and Compounds, 2014, 615: 338–347
34. Gu D D, Dai D H, Chen W H, Chen H Y. Selective laser melting additive manufacturing of hard-to-process tungsten-based alloy parts with novel crystalline growth morphology and enhanced performance. Journal of Manufacturing Science and Engineering, 2016, 138(8): 081003
35. Iveković A, Omidvari N, Vrancken B, Lietaert K, Thijs L, Vanmeensel K, Vleugels J, Kruth J P. Selective laser melting of tungsten and tungsten alloys. International Journal of Refractory Metals and Hard Materials, 2018, 72: 27–32
36. Yves-Christian H, Jan W, Wilhelm M, Konrad W, Reinhart P. Net shaped high performance oxide ceramic parts by selective laser melting. Physics Procedia, 2010, 5: 587–594
37. Attar H, Bönisch M, Calin M, Zhang L C, Scudino S, Eckert J. Selective laser melting of *in situ* titanium–titanium boride composites: processing, microstructure and mechanical properties. Acta Materialia, 2014, 76: 13–22
38. Vrancken B, Thijs L, Kruth J P, Van Humbeeck J. Microstructure and mechanical properties of a novel β titanium metallic composite by selective laser melting. Acta Materialia, 2014, 68: 150–158
39. Chekurov S, Lantela T. Selective laser melted digital hydraulic valve system. 3D Printing and Additive Manufacturing, 2017, 4(4): 215–221
40. Romei F, Grubišić A N, Gibbon D. Manufacturing of a high-temperature resistojet heat exchanger by selective laser melting. Acta Astronautica, 2017, 138: 356–368
41. Ho J Y, Leong K C, Wong T N. Experimental and numerical investigation of forced convection heat transfer in porous lattice structures produced by selective laser melting. International Journal of Thermal Sciences, 2019, 137: 276–287
42. Zhang L, Zhang S S, Zhu H H. Effect of scanning strategy on geometric accuracy of the circle structure fabricated by selective laser melting. Journal of Manufacturing Processes, 2021, 64: 907–915
43. Bai Y C, Zhao C L, Wang D, Wang H. Evolution mechanism of surface morphology and internal hole defect of 18Ni300 maraging steel fabricated by selective laser melting. Journal of Materials Processing Technology, 2022, 299: 117328
44. Aufa A N, Hassan M Z, Ismail Z. Recent advances in Ti–6Al–4V additively manufactured by selective laser melting for biomedical implants: prospect development. Journal of Alloys and Compounds, 2022, 896: 163072
45. Turalıoğlu K, Taftalı M, Yetim F. Determining the tribological behavior of 316L stainless steel with lubricating micro-channels produced by the selective laser melting (SLM) method. Industrial Lubrication and Tribology, 2021, 73(5): 700–707
46. Khan H M, Waqar S, Koç E. Evolution of temperature and

residual stress behavior in selective laser melting of 316L stainless steel across a cooling channel. Rapid Prototyping Journal, 2022, 28(7): 1272–1283

47. Pakkanen J, Calignano F, Trevisan F, Lorusso M, Ambrosio E P, Manfredi D, Fino P. Study of internal channel surface roughnesses manufactured by selective laser melting in aluminum and titanium alloys. Metallurgical and Materials Transactions A, 2016, 47(8): 3837–3844
48. Santhoshsarang D M, Divya K, Telasang G, Soundarapandian S, Bathe R, Padmanabham G. Additively manufactured high-performance conformally cooled H13 tool steel die insert for pressure die casting. Transactions of the Indian National Academy of Engineering, 2021, 6(4): 1037–1048
49. Nagalingam A P, Santhanam V, Dachepally N K G, Yeo S H. Multiphase hydrodynamic flow characterization for surface finishing the laser powder bed fused AlSi10Mg conformal cooling channels. Journal of Manufacturing Processes, 2021, 68: 277–292
50. Qu H Q, Li J, Zhang F C, Bai J M. Anisotropic cellular structure and texture microstructure of 316L stainless steel fabricated by selective laser melting via rotation scanning strategy. Materials & Design, 2022, 215: 110454
51. Maskery I, Aboulkhair N T, Aremu A O, Tuck C J, Ashcroft I A, Wildman R D, Hague R J M. A mechanical property evaluation of graded density Al–Si10–Mg lattice structures manufactured by selective laser melting. Materials Science and Engineering: A, 2016, 670: 264–274
52. Dhiman S, Sidhu S S, Bains P S, Bahraminasab M. Mechanobiological assessment of Ti–6Al–4V fabricated via selective laser melting technique: a review. Rapid Prototyping Journal, 2019, 25(7): 1266–1284
53. Mahmoud D, Al-Rubaie K S, Elbestawi M A. The influence of selective laser melting defects on the fatigue properties of Ti6Al4V porosity graded gyroids for bone implants. International Journal of Mechanical Sciences, 2021, 193: 106180
54. Pei X, Wu L N, Lei H Y, Zhou C C, Fan H Y, Li Z Y, Zhang B Q, Sun H, Gui X Y, Jiang Q, Fan Y J, Zhang X D. Fabrication of customized Ti6Al4V heterogeneous scaffolds with selective laser melting: optimization of the architecture for orthopedic implant applications. Acta Biomaterialia, 2021, 126: 485–495
55. Zhang P, Z. Zhang D, Zhong B. Constitutive and damage modelling of selective laser melted Ti–6Al–4V lattice structure subjected to low cycle fatigue. International Journal of Fatigue, 2022, 159: 106800
56. Maconachie T, Leary M, Lozanovski B, Zhang X Z, Qian M, Faruque O, Brandt M. SLM lattice structures: properties, performance, applications and challenges. Materials & Design, 2019, 183: 108137
57. Echeta I, Feng X B, Dutton B, Leach R, Piano S. Review of defects in lattice structures manufactured by powder bed fusion. The International Journal of Advanced Manufacturing Technology, 2020, 106(5–6): 2649–2668
58. Solyaev Y, Rabinskiy L, Tokmakov D. Overmelting and closing of thin horizontal channels in AlSi10Mg samples obtained by selective laser melting. Additive Manufacturing, 2019, 30: 100847
59. Seharing A, Azman A H, Abdullah S. A review on integration of lightweight gradient lattice structures in additive manufacturing parts. Advances in Mechanical Engineering, 2020, 12(6): 1687814020916951
60. Zhu Y, Zhou L, Wang S, Zhang C, Zhao C, Zhang L, Yang H Y. On friction factor of fluid channels fabricated using selective laser melting. Virtual and Physical Prototyping, 2020, 15(4): 496–509
61. Xiong Y Z, Gao R N, Zhang H, Dong L L, Li J T, Li X. Rationally designed functionally graded porous Ti6Al4V scaffolds with high strength and toughness built via selective laser melting for load-bearing orthopedic applications. Journal of the Mechanical Behavior of Biomedical Materials, 2020, 104: 103673
62. Wally Z J, Haque A M, Feteira A, Claeyssens F, Goodall R, Reilly G C. Selective laser melting processed Ti6Al4V lattices with graded porosities for dental applications. Journal of the Mechanical Behavior of Biomedical Materials, 2019, 90: 20–29
63. Seltzman A H, Wukitch S J. Nuclear response of additive manufactured GRCop-84 copper for use in lower hybrid launchers in a fusion environment. Fusion Engineering and Design, 2020, 159: 111726
64. Liu S Y, Shin Y C. Additive manufacturing of Ti6Al4V alloy: a review. Materials & Design, 2019, 164: 107552
65. Jafari D, Wits W W. The utilization of selective laser melting technology on heat transfer devices for thermal energy conversion applications: a review. Renewable and Sustainable Energy Reviews, 2018, 91: 420–442
66. Yang J X, Wu W L, Wang C L, Liu C G, Wang S Z, Yang D J, Zhou Z, Xu H C. Development status and typical application of selective laser melting technology applications in aerospace field. Journal of Aeronautical Materials, 2021, 41(2): 1–15 (in Chinese)
67. Kirchheim A, Katrodiya Y, Zumofen L, Ehrig F, Wick C. Dynamic conformal cooling improves injection molding. The International Journal of Advanced Manufacturing Technology, 2021, 114(1–2): 107–116
68. Xiao Z F, Yang Y Q, Xiao R, Bai Y C, Song C H, Wang D. Evaluation of topology-optimized lattice structures manufactured via selective laser melting. Materials & Design, 2018, 143: 27–37
69. Langi E, Zhao L G, Jamshidi P, Attallah M M, Silberschmidt V V, Willcock H, Vogt F. Microstructural and mechanical characterization of thin-walled tube manufactured with selective laser melting for stent application. Journal of Materials Engineering and Performance, 2021, 30(1): 696–710
70. Hassanin H, Finet L, Cox S C, Jamshidi P, Grover L M, Shepherd D E T, Addison O, Attallah M M. Tailoring selective laser melting process for titanium drug-delivering implants with releasing micro-channels. Additive Manufacturing, 2018, 20: 144–155
71. Cooper D E, Stanford M, Kibble K A, Gibbons G J. Additive manufacturing for product improvement at red bull technology. Materials & Design, 2012, 41: 226–230
72. Mazur M, Brincat P, Leary M, Brandt M. Numerical and experimental evaluation of a conformally cooled H13 steel injection mould manufactured with selective laser melting. The International Journal of Advanced Manufacturing Technology, 2017, 93(1–4): 881–900

73. Yan C Z, Hao L, Hussein A, Young P. Ti–6Al–4V triply periodic minimal surface structures for bone implants fabricated via selective laser melting. Journal of the Mechanical Behavior of Biomedical Materials, 2015, 51: 61–73
74. Yadroitsev I, Krakhmalev P, Yadroitsava I. Hierarchical design principles of selective laser melting for high quality metallic objects. Additive Manufacturing, 2015, 7: 45–56
75. Tromme E, Kawamoto A, Guest J K. Topology optimization based on reduction methods with applications to multiscale design and additive manufacturing. Frontiers of Mechanical Engineering, 2020, 15(1): 151–165
76. Kimura F, Kadoya S, Kajihara Y. Active air venting of mold cavity to improve performance of injection molded direct joining. Nanomanufacturing and Metrology, 2021, 4(2): 109–117
77. Fang F Z, Gu C Y, Hao R, You K Y, Huang S Y. Recent progress in surface integrity research and development. Engineering, 2018, 4(6): 754–758
78. Stempin J, Tausendfreund A, Stöbener D, Fischer A. Roughness measurements with polychromatic speckles on tilted surfaces. Nanomanufacturing and Metrology, 2021, 4(4): 237–246
79. Urlea V, Brailovski V. Electropolishing and electropolishing-related allowances for powder bed selectively laser-melted Ti–6Al–4V alloy components. Journal of Materials Processing Technology, 2017, 242: 1–11
80. Kruth J P, Froyen L, Van Vaerenbergh J, Mercelis P, Rombouts M, Lauwers B. Selective laser melting of iron-based powder. Journal of Materials Processing Technology, 2004, 149(1–3): 616–622
81. Gu D D, Shen Y F. Balling phenomena during direct laser sintering of multi-component Cu-based metal powder. Journal of Alloys and Compounds, 2007, 432(1–2): 163–166
82. Li R D, Liu J H, Shi Y S, Wang L, Jiang W. Balling behavior of stainless steel and nickel powder during selective laser melting process. The International Journal of Advanced Manufacturing Technology, 2012, 59(9–12): 1025–1035
83. Sing S L, Yeong W Y, Wiria F E, Tay B Y, Zhao Z Q, Zhao L, Tian Z L, Yang S F. Direct selective laser sintering and melting of ceramics: a review. Rapid Prototyping Journal, 2017, 23(3): 611–623
84. Laleh M, Hughes A E, Yang S, Li J L, Xu W, Gibson I, Tan M Y. Two and three-dimensional characterisation of localised corrosion affected by lack-of-fusion pores in 316L stainless steel produced by selective laser melting. Corrosion Science, 2020, 165: 108394
85. Nasab M H, Gastaldi D, Lecis N F, Vedani M. On morphological surface features of the parts printed by selective laser melting (SLM). Additive Manufacturing, 2018, 24: 373–377
86. Shen M Y, Kang C W, Fang F Z. Material removal characteristics of various surface features on selective laser melted 316L stainless steel during electropolishing. Journal of Manufacturing Processes, 2022, 79: 639–653
87. Tian Y, Tomus D, Rometsch P, Wu X H. Influences of processing parameters on surface roughness of Hastelloy X produced by selective laser melting. Additive Manufacturing, 2017, 13: 103–112
88. Bai Y C, Zhao C L, Yang J, Fuh J Y H, Lu W F, Weng C, Wang H. Dry mechanical-electrochemical polishing of selective laser melted 316L stainless steel. Materials & Design, 2020, 193: 108840
89. Bi J, Wu L K, Liu Z Q, Wang H X, Jia X D, Chen X, Starostenkov M D, Dong G J. Formability, surface quality and compressive fracture behavior of AlMgScZr alloy lattice structure fabricated by selective laser melting. Journal of Materials Research and Technology, 2022, 19: 391–403
90. Zhang B C, Lee X H, Bai J M, Guo J F, Wang P, Sun C N, Nai M L, Qi G J, Wei J. Study of selective laser melting (SLM) Inconel 718 part surface improvement by electrochemical polishing. Materials & Design, 2017, 116: 531–537
91. Kumbhar N N, Mulay A V. Post processing methods used to improve surface finish of products which are manufactured by additive manufacturing technologies: a review. Journal of The Institution of Engineers (India): Series C, 2018, 99(4): 481–487
92. Utela B R, Storti D, Anderson R L, Ganter M. Development process for custom three-dimensional printing (3DP) material systems. Journal of Manufacturing Science and Engineering, 2010, 132(1): 011008
93. Butscher A, Bohner M, Roth C, Ernstberger A, Heuberger R, Doebelin N, Rudolf von Rohr P, Müller R. Printability of calcium phosphate powders for three-dimensional printing of tissue engineering scaffolds. Acta Biomaterialia, 2012, 8(1): 373–385
94. Ahn D, Kweon J H, Kwon S, Song J, Lee S. Representation of surface roughness in fused deposition modeling. Journal of Materials Processing Technology, 2009, 209(15–16): 5593–5600
95. Boschetto A, Bottini L, Veniali F. Integration of FDM surface quality modeling with process design. Additive Manufacturing, 2016, 12: 334–344
96. Mohamed O A, Masood S H, Bhowmik J L. Optimization of fused deposition modeling process parameters for dimensional accuracy using I-optimality criterion. Measurement, 2016, 81: 174–196
97. Reddy V, Flys O, Chaparala A, Berrimi C E, V A, Rosen B G. Study on surface texture of fused deposition modeling. Procedia Manufacturing, 2018, 25: 389–396
98. Tronvoll S A, Elverum C W, Welo T. Dimensional accuracy of threads manufactured by fused deposition modeling. Procedia Manufacturing, 2018, 26: 763–773
99. Yasa E, Deckers J, Kruth J P. The investigation of the influence of laser re-melting on density, surface quality and microstructure of selective laser melting parts. Rapid Prototyping Journal, 2011, 17(5): 312–327
100. Newman S T, Zhu Z C, Dhokia V, Shokrani A. Process planning for additive and subtractive manufacturing technologies. CIRP Annals, 2015, 64(1): 467–470
101. Zhu Z C, Dhokia V, Nassehi A, Newman S T. Investigation of part distortions as a result of hybrid manufacturing. Robotics and Computer-Integrated Manufacturing, 2016, 37: 23–32
102. Hur J, Lee K, Zhu-hu, Kim J. Hybrid rapid prototyping system using machining and deposition. Computer-Aided Design, 2002, 34(10): 741–754
103. Maleki E, Bagherifard S, Bandini M, Guagliano M. Surface post-treatments for metal additive manufacturing: progress, challenges, and opportunities. Additive Manufacturing, 2021, 37: 101619
104. Günther J, Leuders S, Koppa P, Tröster T, Henkel S, Biermann

H, Niendorf T. On the effect of internal channels and surface roughness on the high-cycle fatigue performance of Ti–6Al–4V processed by SLM. Materials & Design, 2018, 143: 1–11

105. Leuders S, Meiners S, Wu L, Taube A, Tröster T, Niendorf T. Structural components manufactured by selective laser melting and investment casting—impact of the process route on the damage mechanism under cyclic loading. Journal of Materials Processing Technology, 2017, 248: 130–142
106. Dixit N, Sharma V, Kumar P. Research trends in abrasive flow machining: a systematic review. Journal of Manufacturing Processes, 2021, 64: 1434–1461
107. Guo J, Au K H, Sun C N, Goh M H, Kum C W, Liu K, Wei J, Suzuki H, Kang R K. Novel rotating-vibrating magnetic abrasive polishing method for double-layered internal surface finishing. Journal of Materials Processing Technology, 2019, 264: 422–437
108. Santhosh Kumar S, Hiremath S S. A review on abrasive flow machining (AFM). Procedia Technology, 2016, 25: 1297–1304
109. Han S, Salvatore F, Rech J, Bajolet J, Courbon J. Effect of abrasive flow machining (AFM) finish of selective laser melting (SLM) internal channels on fatigue performance. Journal of Manufacturing Processes, 2020, 59: 248–257
110. Ferchow J, Baumgartner H, Klahn C, Meboldt M. Model of surface roughness and material removal using abrasive flow machining of selective laser melted channels. Rapid Prototyping Journal, 2020, 26(7): 1165–1176
111. Tan K L, Yeo S H, Ong C H. Nontraditional finishing processes for internal surfaces and passages: a review. Proceedings of the Institution of Mechanical Engineers, Part B: Journal of Engineering Manufacture, 2017, 231(13): 2302–2316
112. Ji S M, Cao H Q, Zhao J, Pan Y, Jiang E Y. Soft abrasive flow polishing based on the cavitation effect. The International Journal of Advanced Manufacturing Technology, 2019, 101(5–8): 1865–1878
113. Furumoto T, Ueda T, Amino T, Kusunoki D, Hosokawa A, Tanaka R. Finishing performance of cooling channel with face protuberance inside the molding die. Journal of Materials Processing Technology, 2012, 212(10): 2154–2160
114. Boschetto A, Bottini L, Macera L, Veniali F. Post-processing of complex SLM parts by barrel finishing. Applied Sciences, 2020, 10(4): 1382
115. Khorasani M, Gibson I, Ghasemi A, Brandt M, Leary M. On the role of wet abrasive centrifugal barrel finishing on surface enhancement and material removal rate of LPBF stainless steel 316L. Journal of Manufacturing Processes, 2020, 59: 523–534
116. Łyczkowska E, Szymczyk P, Dybała B, Chlebus E. Chemical polishing of scaffolds made of Ti–6Al–7Nb alloy by additive manufacturing. Archives of Civil and Mechanical Engineering, 2014, 14(4): 586–594
117. Zhang Y F, Li J Z, Che S H, Yang Z D, Tian Y W. Chemical leveling mechanism and oxide film properties of additively manufactured Ti–6Al–4V alloy. Journal of Materials Science, 2019, 54(21): 13753–13766
118. Pyka G, Burakowski A, Kerckhofs G, Moesen M, Van Bael S, Schrooten J, Wevers M. Surface modification of Ti6Al4V open porous structures produced by additive manufacturing. Advanced Engineering Materials, 2012, 14(6): 363–370
119. Han W, Fang F Z. Orientation effect of electropolishing characteristics of 316L stainless steel fabricated by laser powder bed fusion. Frontiers of Mechanical Engineering, 2021, 16(3): 580–592
120. Han W, Fang F Z. Fundamental aspects and recent developments in electropolishing. International Journal of Machine Tools and Manufacture, 2019, 139: 1–23
121. He B, Tian X J, Cheng X, Li J, Wang H M. Effect of weld repair on microstructure and mechanical properties of laser additive manufactured Ti-55511 alloy. Materials & Design, 2017, 119: 437–445
122. Dong G Y, Marleau-Finley J, Zhao Y F. Investigation of electrochemical post-processing procedure for Ti–6Al–4V lattice structure manufactured by direct metal laser sintering (DMLS). The International Journal of Advanced Manufacturing Technology, 2019, 104(9–12): 3401–3417
123. Mingear J, Zhang B, Hartl D, Elwany A. Effect of process parameters and electropolishing on the surface roughness of interior channels in additively manufactured nickel−titanium shape memory alloy actuators. Additive Manufacturing, 2019, 27: 565–575
124. Demir A G, Previtali B. Additive manufacturing of cardiovascular CoCr stents by selective laser melting. Materials & Design, 2017, 119: 338–350
125. Sun Y, Bailey R, Moroz A. Surface finish and properties enhancement of selective laser melted 316L stainless steel by surface mechanical attrition treatment. Surface and Coatings Technology, 2019, 378: 124993
126. Nagalingam A P, Yeo S H. Controlled hydrodynamic cavitation erosion with abrasive particles for internal surface modification of additive manufactured components. Wear, 2018, 414–415: 89–100
127. Tyagi P, Goulet T, Riso C, Stephenson R, Chuenprateep N, Schlitzer J, Benton C, Garcia-Moreno F. Reducing the roughness of internal surface of an additive manufacturing produced 316 steel component by chempolishing and electropolishing. Additive Manufacturing, 2019, 25: 32–38
128. Nagalingam A P, Yuvaraj H K, Santhanam V, Yeo S H. Multiphase hydrodynamic flow finishing for surface integrity enhancement of additive manufactured internal channels. Journal of Materials Processing Technology, 2020, 283: 116692